Numerical Simulation of the Life Cycle of Tropical Cyclones[1]

KATSUYUKI OOYAMA

Geophysical Sciences Laboratory, New York University, Bronx

(Manuscript received 6 May 1968)

ABSTRACT

The tropical cyclone is a solitary creature of the tropical oceans accompanied by violent rotating winds and torrential rain. Observational studies and diagnostic analyses leave little doubt that the energy required for driving the vortex comes from the latent heat of condensation released by tall convective clouds around the center, and that the frictionally induced inflow in the vortex plays a major role in supporting the continued activity of convective clouds. This dual character with respect to important scales of motion poses a great difficulty in investigating the dynamics of tropical cyclones as time-dependent phenomena. However, in order to understand the large-scale aspects of tropical cyclones, one may formulate the role of convective clouds in terms of cyclone-scale variables with only implicit consideration of the dynamics of individual clouds. The present study is an attempt to understand the basic mechanism of tropical cyclones by constructing a numerical-dynamical model on such a basis.

The model assumes that the large-scale hydrodynamical aspects of a tropical cyclone may be represented by an axisymmetric, quasi-balanced vortex in a stably stratified incompressible fluid, while the effects of moist convection may be formulated through the first law of thermodynamics applied to an implicit model of penetrative convective clouds. The air-sea exchange of angular momentum as well as latent and sensible heat is explicitly calculated in the model with the use of conventional approximations.

Results of numerical integration show that the model is capable of simulating the typical life cycle of tropical cyclones, including the mature hurricane stage, with a remarkable degree of reality. The response of the model cyclone to changes in such parameters as the sea surface temperature, the coefficient of air-sea energy exchange, and the initial conditions is tested in a number of numerical experiments to show quite plausible results. A detailed diagnosis of the energy budget of the simulated tropical cyclone is also carried out. The rate of total rainfall, the production and dissipation of kinetic energy, and other energetic characteristics of the computed cyclone compare very well with available estimates for observed tropical cyclones.

Because of the restrictive assumption of axisymmetry and other weak approximations, the model is not realistic enough to predict behavior of individual tropical cyclones in nature. The limitation of the present model in this regard is also discussed.

1. Introduction

Although considerable success has been attained in simulating and predicting the large-scale features of the atmospheric circulation by numerical-dynamical methods, application of similar methods to the tropical cyclone encounters formidable problems associated with the dynamics of moist convection. There is no doubt that the release of condensation heat by tall convective clouds within the storm constitutes the primary energy source to the tropical cyclone. A dynamical model which attempts to simulate the development and maintenance of a tropical cyclone as a time-dependent problem will have to take the energetic role of convective clouds properly into account.

A classical method of incorporating the energy-producing process in a theoretical model of a tropical cyclone was to associate the release of condensation heat directly with the cyclone scale circulation. Under this procedure, the development of a hurricane would not differ in essential mechanisms from that of a cumulonimbus; the only difference would be in the scale of the phenomena. A number of linearized analyses (Haque, 1952; Syōno, 1953; Lilly, 1960; Kuo, 1961; and many others) have been made with this approach, but the results have merely confirmed the rapid growth of cloud-scale convection in the conditionally unstable atmosphere, while yielding little information about tropical cyclones. Of course, the fundamental equations of hydrodynamics and thermodynamics should apply to the entire system of a tropical cyclone. In principle, at least, it should be possible to compute all the clouds along with the evolution of large-scale features, if the grid mesh for numerical integration were chosen to be so fine as to resolve sufficient details of individual convective elements. However, this is a feat neither attractive nor feasible at the present state of the art. Difficulties in this direct line of approach have been well demonstrated in the results of earlier numerical experiments on tropical cyclones by Kashahara (1961), Syōno (1962), and Rosenthal (1964).

Since the development of a tropical cyclone is measured in terms of days and its diameter in terms of

[1] Contribution No. 67 of the Geophysical Sciences Laboratory, Department of Meteorology and Oceanography, New York University.

hundreds of kilometers, the characteristic scales of individual convective clouds, both in time and in horizontal dimensions, are about two orders of magnitude smaller than those of the tropical cyclone. This fact suggests that the dynamics of cumulus convection and the mechanisms governing large-scale features of the tropical cyclone may be treated quite independently. Of course, the two phenomena of different scales are physically not separable; the cyclone-scale circulation depends on the convection for the release of heat energy, while the continued and organized activity of convective clouds in the storm must depend on the large-scale circulation for efficient supply of water vapor. However, for the purpose of studying the tropical cyclone as a large-scale system, it is tempting and probably reasonable to assume that the effects of cumulus convection can be incorporated into a tropical cyclone model without explicit reference to individual clouds.

A crucial problem in this approach is the quantitative formulation of the collective activity and distribution of convective clouds in terms of large-scale field variables, or, as it is commonly called, the parametrization of convective clouds. As a means of formulating the statistical effect of small-scale motions, parametrization is a familiar concept in meteorology. The mixing length theory of eddy transport is a classical example. However, the convective clouds are far more complicated "eddies" than the usual turbulence; first of all, they are energy-producing, and secondly, their vertical extent can be as great as the height of the large-scale system itself. Even a formalistic deduction of statistical properties of convective clouds remains a challenge. At present, therefore, a great degree of reliance on empirical or intuitive hypotheses is unavoidable in developing a parametrized formulation of implicit convection. The use of such devices does not free research on tropical cyclones from the need for further progress in the study of convective clouds. However, it may allow the two fields of study to proceed in parallel. Besides the cumulus convection, there are many other problems to be considered in order to understand the tropical cyclone as a large-scale system.

A conceptual trend toward the new type of tropical cyclone models with implicit convection had already been developing among theoretical investigators (e.g., Yanai, 1961), when the first specific proposals of such a model were presented by the writer[2] and by Charney and Eliassen (1964). Linearized perturbation analyses of these two models led essentially to the same conclusion that intensification of a weak tropical disturbance with an e-folding time of a few days could be explained as a positive feedback process between the increased cyclone circulation and the increased supply of warm, moist air into the convective region by the frictionally induced inflow. However, the numerical integration of the model by the writer (Ooyama, 1964) failed to simulate the mature stage of a tropical cyclone in that the computed vortex did not stop growing. The numerical integration of Charney and Eliassen's model by Ogura (1964) produced almost identical results. Another model with elaborate hypotheses on the implicit cumulus convection was proposed by Kuo (1965). The numerical integration of this model appeared to produce a steady state but the computed cyclones were quite unlike those observed in nature. However, it may be said, in spite of all the shortcomings of their first attempts, that these models have opened a promising new approach to numerical simulation of the tropical cyclone.

The tropical cyclone model proposed in this paper is an improved version of the author's earlier model. As before, the hydrodynamical aspects of cyclone circulation are approximated by an axisymmetric balanced vortex in three layers of incompressible fluid. The bottom layer represents the planetary boundary layer, and the other two the stably stratified free atmosphere. The air-sea exchange of angular momentum and thermodynamical energy is formulated through conventional approximations. Major improvements over the earlier model are introduced in the parametrization of implicit convective clouds. The parameter η, representing a measure of instability of deep convection and previously considered to be constant, is now variable and takes into account the stabilizing effect of the warm core as well as the variation of equivalent potential temperature in the boundary layer.

The tropical cyclone simulated with the present model does not approach a steady state. (There is no positive evidence that a tropical cyclone should or could attain a steady state, although omission of local time derivatives is frequently justifiable for diagnostic purposes.) In a typical case of simulation, a weak disturbance rapidly grows into an intense but relatively small vortex after a period of indecisive self-organization. As a warm core is gradually established with the intensification of cyclonic circulation, the moist static stability near the center approaches an almost neutral state. This reduction of convective instability checks further intensification in terms either of the maximum wind speed or of the central surface pressure. However, the area of hurricane force winds continues to expand several more days after the intensity has reached a peak. This general behavior of the simulated cyclone is in good agreement with the typical behavior of real tropical cyclones in the formative, deepening (immature) and mature stages (Riehl, 1954).

For the purpose of understanding the basic mechanisms of the tropical cyclone, it is instructive to examine

[2] Ooyama, K.: A dynamical model for the study of tropical cyclone development. Unpubl. manuscript prepared for presentation at the 43rd annual meeting of the American Meteorological Society, New York, January 1963. Preliminary results of numerical experiments were presented at the Intern. Symp. on Numerical Weather Forecasting, Oslo, March 1963. Because of unsatisfactory numerical results, the work has not been published except in a short paper (Ooyama, 1964). Although the writer was unaware until 1963, J. G. Charney had been publicly lecturing on the idea of collective, frictionally controlled dynamics since 1956.

the response of the computed cyclone to changes in various physical parameters. A considerable variation of cyclone intensity in response to small changes in the sea surface temperature, as well as the rapid decay of the cyclone at simulated landfall, is found to be quite realistic. Results of these and other experiments indicate that the supply of latent heat from the ocean under the direct influence of a tropical cyclone is extremely important to both development and maintenance of the cyclone. The rate of total rainfall, the production and dissipation of kinetic energy, and other energetic characteristics are computed for the simulated cyclone. The results compare very well with available estimates for observed tropical cyclones.

There are obvious restrictions on what can be investigated with the present model. Under the assumption of axisymmetry, it is not possible to consider the movement of the cyclone center or to investigate the interaction of the cyclone with the synoptic environment. Furthermore, the limited accuracy of various approximations adds to uncertainty in the quantatitive verification of the model performance. No attempt is made to simulate any particular tropical cyclone in nature. However, it is hoped that the present study may serve as a stepping stone to construction of better models with which prediction of real tropical cyclones may some day become possible.

2. The fluid system

A conventional way of deriving a numerical model is to begin with the governing equations in the differential form, and then to introduce their finite difference analogues at a later stage. With the use of sufficiently small increments for time and spatial coordinates, the discretization of continuous variables and their derivatives may be considered as a matter of computational approximation. However, the situation is different in the case of a tropical cyclone model in which the effect of moist convection is formulated in terms of cyclone-scale variables without explicitly recognizing individual convective clouds. Although the characteristic time and horizontal scales of convective clouds are both very much smaller than those of the tropical cyclone, the vertical scale of tall convective clouds is about the same as that of the cyclone itself. If this fact is duly emphasized in the so-called parametrization of moist convection, the resulting formulas will contain integral relations for the vertical column and will not be written entirely in differential relations with respect to the vertical coordinate. Therefore, the meaningful vertical resolution of a particular formulation is more likely to depend on the number of independent integral relations derived from physical hypotheses on moist convection than on the number of layers in the vertical chosen for numerical accuracy.

Besides the difficulty in formulating the moist convection on a largely intuitive basis (see Section 5), there is a considerable amount of uncertainty in our knowledge about other physical processes contributing to a tropical cyclone. At present, therefore, we may try to construct only a minimum model with which various ideas concerning the basic dynamical aspects of a tropical cyclone could be tested with the least amount of mathematical complexity. For this purpose, we shall approximate the cyclone-scale motion fields of a tropical cyclone by a quasi-balanced axisymmetric vortex (see Section 3), allowing, however, only two degrees of freedom to describe vertical distribution of the tangential circulation and one degree of freedom to represent the temperature of a vertical column. Then, the diabatic heating by convective clouds may be formulated only in terms of the mean effect on the column.

In the construction of a numerical model of such a low vertical resolution, the discretization procedure requires careful attention in order to insure that the energy and other integral properties of the system of finite difference equations are physically consistent. One method frequently adopted to simplify this problem is the replacement of the atmosphere by a few layers of incompressible homogeneous fluid. In the case of large-scale motions in a stably stratified atmosphere, the incompressible fluid system is dynamically similar to the atmospheric system if the specific volume is interpreted to be analogous to the potential temperature.

One obvious reason for the simplicity of the incompressible fluid system is the absence of true thermodynamics. While this peculiarity is not a serious problem for a study of adiabatic motions in the atmosphere, it may present a difficulty in interpretation if an attempt is made to introduce diabatic processes into the system. In the present study, however, the major diabatic process is associated with unstable moist convection which, for reasons of its own, will require an indirect formulation. In this special situation, the use of an incompressible fluid system does not prove to be a critical disadvantage because the explicit part of the model represents only the cyclone-scale fields which undergo adiabatic changes. Therefore, partly for reasons of continuity with the author's earlier work, and partly for simplicity in deriving a consistent system of equations of low-order vertical resolution, the incompressible-fluid approximation of the atmosphere will be adopted in this study.

The fluid system of the model is assumed to consist of two main layers of incompressible homogeneous fluid and an additional thin layer at the bottom, adjacent to the sea surface. In the following, the numerical subscripts 0, 1 and 2 will refer to the bottom layer, the lower main layer, and the upper main layer, respectively. A schematic diagram of the model is shown in Fig. 1. The thickness of each main layer, h_1 or h_2, is variable and is a function of time t and radius r under the axisymmetry assumption. The density of each layer, ρ_1 or ρ_2, is constant, but, in order to represent the stable stratification of the troposphere, we assume the

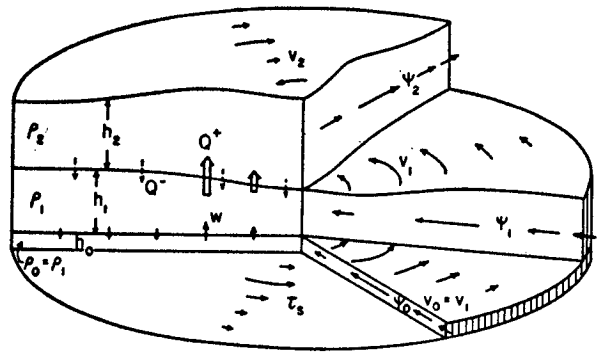

FIG. 1. Schematic diagram depicting the basic design of the model.

density ratio ϵ to be less than unity, i.e.,

$$\epsilon=\rho_2/\rho_1<1. \tag{2.1}$$

The top of the upper main layer is assumed to be a free surface. For the bottom layer, which represents the planetary boundary layer (or Ekman boundary layer), we simply assume both that the thickness h_0 is a given constant and that $\rho_0=\rho_1$.

As will become clear, the absolute value of density in this model is only an important factor when the magnitudes of certain quantities such as the sea surface pressure, the total kinetic energy, etc., are compared with observed values. Therefore, if we introduce a constant reference density ρ and write

$$\rho_0=\rho_1=\rho \quad \text{and} \quad \rho_2=\epsilon\rho, \tag{2.2}$$

we may eliminate the appearance of ρ from most of the equations in the rest of the paper. Then, the effect of the density stratification will be represented by either the ratio ϵ or a nondimensional measure of static stability σ, defined by

$$\sigma=1-\epsilon=(\rho_1-\rho_2)/\rho_1. \tag{2.3}$$

Since the specific volume of a stratified incompressible fluid is analogous to the potential temperature, the density of an individual fluid parcel should remain constant during motion representing the adiabatic motion in the atmosphere. However, adiabatic changes of temperature may be considered as being represented by variations of the thicknesses h_1 and h_2, due to horizontal convergence or divergence of fluid in the main layers. Under the axisymmetry assumption, only the radial motion contributes to the divergence. It will be convenient to express the radial motion in terms of radial flux ψ_j ($j=0, 1, 2$), defined by

$$\left.\begin{aligned}\psi_0&=-h_0u_0r\\ \psi_1&=-h_1u_1r\\ \psi_2&=-\epsilon h_2u_2r\end{aligned}\right\}, \tag{2.4}$$

where u_j is the radial component (positive outward) of fluid velocity in the respective layer. When ψ_j is multiplied by the common factor ρ, the product

$$\rho\psi_j=-\rho_jh_ju_jr,$$

represents the total inward mass flux across the entire thickness of each layer per unit radian of arc at radius r. However, there will be little confusion if we call ψ_j itself the radial mass flux.

In contrast to the density-conserving "adiabatic" motion, diabatic processes should be represented by changes in density of individual fluid parcels, as they are associated in the atmosphere with vertical motions relative to isentropic surfaces. Since the density is assumed to take only two discrete values, the diabatic heating in a unit column may be represented in this model by a vertical mass flux, ρQ^+, across the interface per unit horizontal area from the lower layer of density ρ_1 to the upper layer of the smaller density ρ_2. Similarly, the diabatic cooling in a unit column may be represented by a vertical mass flux, ρQ^-, across the interface in the opposite direction. By definition, Q^+ and Q^-, which we may call the diabatic mass fluxes (again disregarding the constant ρ), have the physical dimension of velocity. However, these fluxes do not represent the vertical velocity of fluid since the interface itself can move. Specification of the diabatic mass fluxes in terms of other model variables constitutes one of the most crucial problems in the present study. A full discussion of this question will be given in Sections 5, 6 and 7.

Since the thickness of the boundary layer is assumed to be a constant, the equation of continuity for this layer is

$$0=\frac{\partial\psi_0}{r\partial r}-w, \tag{2.5}$$

where w denotes the vertical velocity at the top of the boundary layer. The equation of continuity for each of the main layers, including the mass exchange with adjacent layers, is given by

$$\left.\begin{aligned}\frac{\partial h_1}{\partial t}&=\frac{\partial\psi_1}{r\partial r}-Q+w\\ \epsilon\frac{\partial h_2}{\partial t}&=\frac{\partial\psi_2}{r\partial r}+Q\end{aligned}\right\}, \tag{2.6}$$

where Q, the net diabatic flux, is

$$Q=Q^+-Q^-. \tag{2.7}$$

Under the hydrostatic approximation, the pressure p_j in the main layers ($j=1$ and 2) is given by

$$\left.\begin{aligned}p_1&=g\rho(h_0+h_1+\epsilon h_2-z)\\ p_2&=\epsilon g\rho(h_0+h_1+h_2-z)\end{aligned}\right\}, \tag{2.8}$$

where g is the acceleration of gravity and z the height above the sea level. The pressure p_0 in the boundary

layer is given by the same formula as p_1. If we denote a standard thickness of each layer (i.e., the undisturbed value of h_j at a sufficiently large radius) by $\bar{h}_j$, and the corresponding standard pressure by $\bar{p}_j$, we may define another dependent variable,

$$\phi_j=(p_j-\bar{p}_j)/\rho_j,$$

or more specifically,

$$\left.\begin{aligned}\phi_1&=g\{(h_1-\bar{h}_1)+\epsilon(h_2-\bar{h}_2)\}\\ \phi_2&=g\{(h_1-\bar{h}_1)+(h_2-\bar{h}_2)\}\end{aligned}\right\}. \tag{2.9}$$

Evidently, ϕ_j is the deviation of the geopotential of an isobaric surface from its standard value at large radius. Although p_j and $\bar{p}_j$ depend on z, ϕ_j does not; it is a function only of r and t. We may similarly define ϕ_0 for the boundary layer but, obviously,

$$\phi_0=\phi_1. \tag{2.10}$$

3. The equations of motion

It will be assumed that the tangential circulation of the model cyclone is represented by a balanced axisymmetric vortex. Let v_j denote the tangential component of velocity (positive counterclockwise). This condition of balance, which substitutes for the radial equation of motion, is given for each layer ($j=0, 1, 2$) by the gradient wind equation

$$\left(f+\frac{v_j}{r}\right)v_j=\frac{\partial\phi_j}{\partial r}, \tag{3.1}$$

where f, the Coriolis parameter, is assumed to be constant. From (2.10) and the above assumption, it follows that

$$v_0=v_1. \tag{3.2}$$

The use of the diagnostic relation (3.1) in a time-dependent problem implies that time variations of the tangential circulation and mass fields are so slow that the two fields are always in a state of quasi-static equilibrium. The balance approximation in this sense was first introduced by Eliassen (1952), and has been applied in a more general form to studies of large-scale atmospheric motions. In order to apply the approximation to tropical cyclones, a few further remarks may be in order.

It has been suggested by earlier investigators that hydrodynamic instability is involved in the formation of a tropical cyclone from a weak vortex; for example, instability of a purely inertial type was proposed by Sawyer (1947), and baroclinic instability by Kleinschmidt (1951) and Yanai (1961). If these types of hydrodynamic instability were really necessary to account for the formation of an intense cyclone, the balance approximation could not be employed in the present study. Yanai (1961, 1964) showed that purely inertial instability is too weak to play a major role in the formation, but he emphasized the probable importance of baroclinic instability in explaining the rapid development of a tropical cyclone which, according to his analysis, occurred after the establishment of a warm core due to organized cumulus convection in an incipient vortex. However, there is little observational evidence that a baroclinically unstable region, if it existed, would be so widespread as the instability theory assumed. Furthermore, a rigorous discussion of the baroclinic instability criteria by Ooyama (1966) showed that the sudden onset of unstable development in the manner proposed by Yanai (1961) was theoretically improbable. Therefore, if there is any doubt about the use of the balance approximation in the present study, it is likely to concern not the principle, but only the degree of accuracy of the approximation. In regard to the latter, further comment will be given in the discussion of the boundary layer approximation below.

The absolute angular momentum M_j about the vertical axis per unit mass of fluid in each layer ($j=0, 1, 2$) is defined by

$$M_j=v_jr+\tfrac{1}{2}fr^2, \tag{3.3}$$

and, because of (3.2),

$$M_0=M_1. \tag{3.4}$$

Then the angular momentum budget in the main layers may be written in the form

$$\left.\begin{aligned}\frac{\partial}{\partial t}(h_1M_1)&=\frac{\partial}{r\partial r}(\psi_1M_1+\Lambda_1)-Z_{12}+Z_{01}\\ \epsilon\frac{\partial}{\partial t}(h_2M_2)&=\frac{\partial}{r\partial r}(\psi_2M_2+\Lambda_2)+Z_{12}\end{aligned}\right\}. \tag{3.5}$$

In the above, Λ_1 and Λ_2 are the radial flux of angular momentum due to lateral eddy transport per unit radian of arc in each of the main layers (positive inward in accordance with the sign convention for the radial advective fluxes) and may be evaluated from

$$\left.\begin{aligned}\Lambda_1&=\lambda_1h_1r^3\frac{\partial}{\partial r}\left(\frac{v_1}{r}\right)\\ \Lambda_2&=\epsilon\lambda_2h_2r^3\frac{\partial}{\partial r}\left(\frac{v_2}{r}\right)\end{aligned}\right\}, \tag{3.6}$$

where λ_1 and λ_2 are the (kinematic) coefficients of eddy viscosity. The vertical flux of angular momentum, per unit horizontal area, across the interface between the main layers is denoted by Z_{12}. It consists of the advective transport by the diabatic mass fluxes and the transfer by the shearing stress at the interface. If we assume the stress to be expressed in a linear form with a coefficient μ, we may write Z_{12} as

$$Z_{12}=M_1Q^+-M_2Q^-+\mu(M_1-M_2). \tag{3.7}$$

The vertical flux of angular momentum from the boundary layer to the lower main layer is denoted by Z_{01}. Because of (3.4), it consists only of the advective flux and is given by

$$Z_{01}=M_1 w. \tag{3.8}$$

The angular momentum budget of the planetary boundary layer could be written in a similar form to (3.5). However, if the thickness h_0 of the layer is sufficiently small compared to the thickness of the main layers, the local time change of the angular momentum may be neglected in comparison to the net advective change or the frictional transfer to the sea. Then, again because of (3.4), we may write

$$\frac{\partial}{r\partial r}(M_1\psi_0)-Z_{01}+Z_s=0, \tag{3.9}$$

where Z_s is the angular momentum flux at the sea surface or the torque exerted by the sea on the air (apart from the factor ρ). If τ_s denotes the tangential component of shearing stress at the sea surface, Z_s is written as

$$Z_s=-\tau_s r/\rho, \tag{3.10}$$

and τ_s itself may be given by

$$\tau_s=\rho C_D|v_1|v_1, \tag{3.11}$$

where C_D is the drag coefficient. The fact that the wind speed near the sea surface is generally smaller than the gradient wind $v_1(=v_0)$ can be roughly taken into account if the drag coefficient, which is usually determined for the anemometer level wind, is adjusted for the gradient wind. The use of $|v_1|$ in (3.11), instead of the magnitude of vector wind, is a minor simplification if one considers the uncertainty in our present knowledge of the dependency of C_D itself on the wind speed. The precise specification of C_D assumed in the numerical experiments will be given in Section 9. The radial eddy flux of angular momentum could have been included in (3.9). However, its effect on the angular momentum budget is relatively minor even in the main layers and is probably more so in the boundary layer.

The omission of the local time derivative in (3.9) considerably simplifies the numerical computations but it is by no means a necessary or critical assumption of the present model. Whether the time derivative is omitted or not, a more serious concern about the accuracy of (3.9) stems from the use of the balance approximation (3.1) in the boundary layer, from which (3.2) and (3.4) automatically follow. As shown in a scale analysis by Ogura (1964), the gradient wind relationship holds fairly well in the free atmosphere, but does not necessarily do so in the planetary boundary layer under hurricane force winds. Both Ogura (1964) and Kuo (1965), who nevertheless tried the balance approximation in their numerical experiments, emphasized the weakness of the approximation as one of the reasons for certain unsatisfactory aspects of their results. However, numerical results of the present study indicate that the balance approximation is not as detrimental as the previous authors have implied. It is possible to eliminate the balance approximation from the boundary layer formulation by the use of more accurate diagnostic equations. (Numerical testing of such a formulation is currently under way.) At present, however, there are many other basic problems to be understood concerning the dynamics of tropical cyclones. The balance approximation still appears to be a useful simplification.

The prognostic equations (2.6) and (3.5), and the related diagnostic equations (2.5) and (3.9), have been given in the so-called conservation form in order to assure consistency in the mass and angular momentum budget. For further discussion, it is convenient to transform those equations in the following way. By differentiating (2.9) with respect to time and eliminating $\partial h_j/\partial t$ from (2.6), the prognostic equations for ϕ_j $(j=1, 2)$ may be obtained as

$$\left.\begin{aligned}\frac{\partial\phi_1}{\partial t}&=g\frac{\partial}{r\partial r}(\psi_1+\psi_2)+G_1\\ \frac{\partial\phi_2}{\partial t}&=g\frac{\partial}{r\partial r}(\psi_1+\epsilon^{-1}\psi_2)+G_2\end{aligned}\right\}, \tag{3.12}$$

where

$$\left.\begin{aligned}G_1&=gw\\ G_2&=g(w+\epsilon^{-1}\sigma Q)\end{aligned}\right\}. \tag{3.13}$$

Once ϕ_j is predicted, h_j may be determined by solving (2.9); that is,

$$\left.\begin{aligned}h_1&=\bar{h}_1+(\sigma g)^{-1}(\phi_1-\epsilon\phi_2)\\ h_2&=\bar{h}_2+(\sigma g)^{-1}(-\phi_1+\phi_2)\end{aligned}\right\}. \tag{3.14}$$

By combining (2.6) with (3.5), the prognostic equations for v_j may be obtained as

$$\left.\begin{aligned}\frac{\partial v_1 r}{\partial t}&=h_1^{-1}(f+\zeta_1)\psi_1+F_1\\ \frac{\partial v_2 r}{\partial t}&=(\epsilon h_2)^{-1}(f+\zeta_2)\psi_2+F_2\end{aligned}\right\}, \tag{3.15}$$

where

$$\left.\begin{aligned}F_1&=\frac{1}{h_1}\left\{(Q^-+\mu)(v_2-v_1)r+\frac{\partial\Lambda_1}{r\partial r}\right\}\\ F_2&=\frac{1}{\epsilon h_2}\left\{(Q^++\mu)(v_1-v_2)r+\frac{\partial\Lambda_2}{r\partial r}\right\}\end{aligned}\right\}, \tag{3.16}$$

and, for $j=1$ and 2,

$$\zeta_j=\frac{\partial v_j r}{r\partial r}. \tag{3.17}$$

Eqs. (2.5) and (3.9) for the boundary layer may be written simply as

$$w=\frac{\partial\psi_0}{r\partial r}, \tag{3.18}$$

and

$$\psi_0=(f+\zeta_1)^{-1}C_D|v_1|v_1 r. \tag{3.19}$$

4. The compatibility condition and radial fluxes

In order to predict ϕ_j and v_j ($j=1, 2$) with (3.12) and (3.15), we must know the radial fluxes ψ_1 and ψ_2. However, the radial fluxes cannot be specified by introducing additional independent equations because the predicted fields of ϕ_j and v_j must satisfy the balance condition (3.1). In other words, the transverse circulation must be determined in such a way that the prognostic equations are compatible with the balance hypothesis. By differentiating (3.1) with respect to time and then eliminating time derivatives with substitution from (3.12) and (3.15), the required condition for compatibility is obtained in the form

$$\left.\begin{aligned} r\frac{\partial}{\partial r}\left\{\frac{\partial}{r\partial r}(\psi_1+\psi_2)\right\}-S_1\psi_1=B_1 \\ r\frac{\partial}{\partial r}\left\{\frac{\partial}{r\partial r}(\psi_1+\epsilon^{-1}\psi_2)\right\}-\epsilon^{-1}S_2\psi_2=B_2 \end{aligned}\right\}, \tag{4.1}$$

where, for $j=1, 2$,

$$S_j=\left(f+\frac{2v_j}{r}\right)\left(\frac{f+\zeta_j}{gh_j}\right), \tag{4.2}$$

$$B_j=-\frac{1}{g}\left\{\left(f+\frac{2v_j}{r}\right)F_j-r\frac{\partial}{\partial r}G_j\right\}. \tag{4.3}$$

In the above, S_j is a measure of the inertial stability against radial displacements in each layer, and B_j may be considered as the forcing term due to redistribution of angular momentum F_j and mass G_j by friction and diabatic processes. The static stability of the fluid system is hidden in the coefficient matrix of the terms in parentheses on the left-hand side of (4.1).

In order to solve (4.1) for ψ_1 and ψ_2, appropriate boundary conditions must be given at the center, $r=0$, and at a sufficiently large radius, $r=r_x$. However, if both B_1 and B_2 vanish at the center as is the case here, it is sufficient to require that

$$\psi_1=\psi_2=0 \quad \text{at} \quad r=0. \tag{4.4}$$

As for the outer boundary condition, it may be ideal to require the fluxes to vanish at an infinite radius. However, for the reason of computational economy, numerical calculations in this study are carried out only up to $r_x=1000$ km. Since this radius is very nearly the Rossby radius of internal deformation (see below), an appreciable amount of distortion in numerical results might be expected during a long-term integration of the model (say, for several days) if the fluid system were assumed to be closed at 1000 km by allowing no fluxes across the boundary. In order to alleviate a false influence of the computational boundary, the system is assumed to be open at r_x under the boundary conditions

$$\left.\begin{aligned} \psi_0+\psi_1+\psi_2=0 \\ \frac{\partial\psi_2}{\partial r}=-\frac{\psi_2}{R} \end{aligned}\right\} \quad \text{at} \quad r=r_x, \tag{4.5}$$

where R is a constant parameter with the dimension of length.

Although the first condition of (4.5) implies no net mass flux at $r_x=1000$ km, the inflow and outflow are not required to vanish individually. However, since the forcing terms in (4.1) are expected to be very small outside r_x, the radial fluxes should decrease with increasing radius. If the curvature effect of polar coordinates is neglected, the decrease can be shown (Bolin, 1953) to be proportional to $\exp(-r/\bar{R})$, where the scale factor $\bar{R}$ may be called, in analogy with Rossby (1938), the radius of (internal) deformation and is defined in the present model (assuming $\bar{h}_1=\bar{h}_2\equiv\bar{h}$) by

$$\bar{R}=(\sigma g\bar{h}/2)^{\frac{1}{2}}f^{-1}. \tag{4.6}$$

Then, in order to match the interior solution of (4.1) with the exponential solution outside r_x, we may choose $R=\bar{R}$ in (4.5). In the case of axisymmetry, a similar argument yields

$$R=\bar{R}K_1(r_x/\bar{R})\{K_0(r_x/\bar{R})\}^{-1}, \tag{4.7}$$

where K_0 and K_1 are the modified Bessel function of order 0 and 1, respectively. A typical choice of the model parameters (Section 9) gives $\bar{R}=1000$ km and $R=1400$ km.

Being forced by effects of friction and diabatic processes, the balanced vortex (3.1) undergoes a continuous transition from one state of equilibrium to another. The solutions ψ_1 and ψ_2 of (4.1) under the boundary conditions (4.4) and (4.5) represent radial adjustments required by such a transition. As was discussed by Eliassen (1952), the successive states of equilibrium must be stable ones if the concept of "quasi-static" adjustment is to be applicable. In other words, the pair of solutions ψ_1 and ψ_2 of the boundary value problem should be unique so that no transverse circulation is possible without the forcing terms.

Suppose, tentatively, that two distinct pairs of solutions, (ψ_1,ψ_2) and (ψ_1',ψ_2'), exist satisfying the same equation (4.1) and the same boundary conditions (4.4) and (4.5). Let us denote the difference $\psi_1-\psi_1'$ by Ψ_1 and $\psi_2-\psi_2'$ by Ψ_2. Then, with some mathematical manipulation, it can be shown that Ψ_1 and Ψ_2 satisfy

the integral relation

$$\int_0^{r_x}\left\{\left(\frac{\partial\Psi_1}{\partial r}+\frac{\partial\Psi_2}{\partial r}\right)^2+\frac{\sigma}{\epsilon}\left(\frac{\partial\Psi_2}{\partial r}\right)^2+S_1\Psi_1^2+\frac{S_2}{\epsilon}\Psi_2^2\right\}\times\frac{dr}{r}+\frac{\sigma}{\epsilon R}\left(\frac{\Psi_2}{r}\right)^2_{r=r_x}=0. \quad (4.8)$$

Therefore, if it holds everywhere that

$$S_1\geqslant 0 \quad \text{and} \quad S_2\geqslant 0, \quad (4.9)$$

both Ψ_1 and Ψ_2 must be identically zero; that is, the original pair of solutions (ψ_1,ψ_2) are unique.

It has been found in numerical integration of the present model that S_2 becomes negative in a region at some distance from the center because the absolute vorticity in the upper layer, $f+\zeta_2$, becomes negative there. However, no computational difficulty in solving the boundary value problem for ψ_1 and ψ_2 has been experienced. Mathematically, this is not surprising, since (4.9) is by no means a necessary condition for the uniqueness but merely a sufficient one. Indeed, with the use of the Schwartz inequality to estimate the integral, it can be shown that (4.8) requires both Ψ_1 and Ψ_2 to vanish everywhere in the interval of integration even if S_2 takes negative values in part of the interval, provided that the magnitude and the radial extent of negative S_2 are limited. Nevertheless, the apparent stability in computation may appear paradoxical since the negative absolute vorticity implies the possibility of inertial instability. The reason for the stability is the low degree of freedom in the representation of motion fields in this model. Even if the radial motion in the region of negative absolute vorticity tended toward unstable acceleration, unstable displacements alone could not possibly occur under the imposed constraint of the axisymmetric two-layer model; such displacements would have to be accompanied by displacements in other regions, especially in the lower layer, against inertial and static stability. Therefore, unless the negative vorticity becomes very intense and widespread, the basic mode of transverse circulation can remain stable.

If the assumption of axisymmetry were removed and the vertical resolution were increased, the inertial instability could locally generate small-scale motions to which the balance approximation might not be applicable. The observed outflow in the upper troposphere at a few hundred kilometers from the center of a tropical cyclone often shows marked streakiness or breaks up into a number of anticyclonic cells (Jordan, 1952). Such deviations from axisymmetric motion may possibly increase the eddy transport of angular momentum in the outflow region, although the effect on the behavior of a tropical cyclone as a whole is not known for certain. However, as far as the basic driving mechanism of a tropical cyclone is concerned, the observed degree of inertial instability is much too weak to be of primary importance (Yanai, 1964). This fact is consistent with our experience that the negative absolute vorticity computed in cyclones with the model did not become so intense as to contradict the balance hypothesis.

5. Modeling of cumulus convection

If cumulus convection were to be formulated directly from first principles of hydrodynamics and thermodynamics, we would face the unattractive, if not impossible, prospect of computing numerous convective clouds within a single mathematical model of the tropical cyclone. Therefore, as discussed earlier, we shall incorporate in this model only the collective effects of implicit cumulus convection, even though this approach requires, at present, the use of empirical or intuitive hypotheses concerning the behavior of individual clouds.

The need for incorporating effects of cumulus convection in this approximate manner is not limited to studies of the tropical cyclone. In large-scale weather systems, as well, convective clouds not only act as heat sources but also render an effective means of transporting heat upward. In order to introduce these effects into their general circulation models, Mintz (1965), Smagorinsky *et al.* (1965), and Manabe *et al.* (1965) have formulated various ways of adjusting the temperature lapse rate at places where large-scale conditions are favorable for moist convection. These hypotheses of convective adjustment have the virtue of easy application to a multi-level model, since the adjustment is *essentially* based on the moist stability at each level as locally determined from the large-scale fields of temperature and moisture.

In the tropics, however, cumulus clouds are frequently observed to rise to upper levels of the troposphere, penetrating through a deep layer of relatively dry air. The moist instability responsible for such convection is not the local one between adjacent levels, but the instability of the low-level air rising through the deep layer above. By reducing the critical humidity (in the large-scale sense) to less than 100% the convective adjustment hypothesis may be modified to meet the prevailing situation in the tropics. However, by emphasizing the penetrative nature of convective clouds much further, it is possible to formulate a different hypothesis on moist convection which is more suitable for application to studies of tropical cyclones.

For this purpose, we first examine typical thermal and moisture stratifications of the tropical atmosphere as shown in Fig. 2. The potential temperature θ and the equivalent potential temperature θ_e in this figure are based on summer mean data over the West Indies after Jordan (1958). The third curve, θ_e^*, shows the vertical distribution of the equivalent potential temperature which the air would possess if it were saturated with water vapor at the same temperature at each level. The notable features of this atmosphere are the relatively

high values of θ_e in the planetary boundary layer (the lowest kilometer), and the sharp decrease of θ_e with height above the boundary layer.

Suppose that a parcel of air is lifted pseudo-adiabatically from the boundary layer. If the path of the parcel in terms of θ_e were shown in Fig. 2, it would be a straight vertical line starting from a representative point (say, at 950 mb) on the θ_e curve. Condensation of water vapor will begin before this path intersects the θ_e^* curve, and the parcel will become warmer than the ambient air above the point of intersection. The parcel, then, will be accelerated by its buoyancy and continue to rise toward the tropopause or beyond. Of course, pseudo-adiabatic ascent of a parcel without mixing is unlikely to occur; a more realistic path of the parcel, which is mixed with ambient air as it rises, will be much closer to the θ_e^* curve than to the vertical straight line. On the other hand, if a parcel of air in the free atmosphere (above the 900-mb level) is lifted pseduo-adiabatically, its equivalent potential temperature will follow a vertical path which does not intersect the θ_e^* curve. Thus, even though condensation may occur, the parcel will never become warmer than the ambient air. Therefore, the possibility of unstable moist convection in this atmosphere depends critically on the high values of θ_e in the boundary layer. The moisture in the free atmospheric air may contribute to moist convection, rather passively, only when the air is entrained into the updraft driven by the excess buoyancy of the air from the boundary layer.

The stratification in a tropical cyclone is not necessarily the same as the mean state shown in Fig. 2. However, it is still generally true that the mid-tropospheric air is not convectively unstable. Furthermore, what we are concerned with in this study is organized convective activity for a period much longer than the time scale of individual convective clouds. In order to support such activity, it is apparently necessary for the boundary layer inflow to converge, so that convectively unstable air will be continuously supplied to the convective clouds.

Charney and Eliassen (1964) and Kuo (1965) have assumed, in their tropical cyclone models, that convective activity will occur if convergence of the advective flux of water vapor at every level plus evaporative supply from the sea surface tends to increase the total water vapor content in a unit vertical column. Since this hypothesis does not distinguish between the equivalent potential temperatures at different levels, it may allow convective activity to occur by convergence of the convectively stable, mid-tropospheric air. However, this possibility is unlikely to occur in nature, since the major contribution to the total convergence of water vapor in a vertical column should come from the convergence in the boundary layer, in which case the criterion above becomes practically the same as the one employed in this study. It is also unlikely that convective activity in a column would be supported mainly by

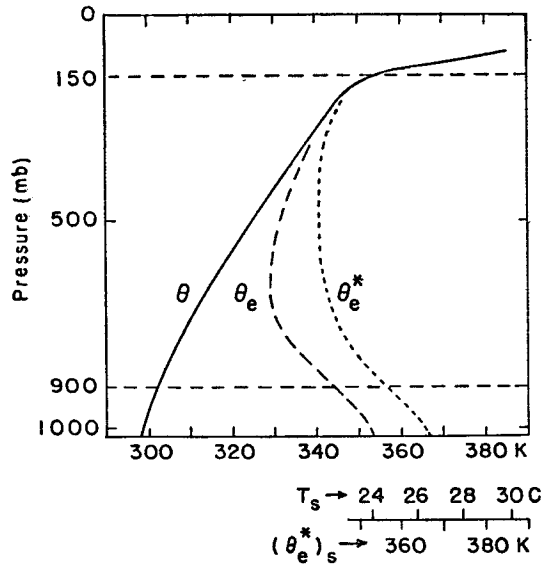

FIG. 2. Typical stratification of the tropical atmosphere (after Jordan, 1958) where θ is the potential temperature, θ_e the equivalent potential temperature, θ_e^* the equivalent potential temperature of the hypothetically saturated air of the same temperature at each level. Correspondence between the sea surface temperture T_s and the saturated equivalent potential temperature, $(\theta_e^*)_s$ at the sea surface, is shown on the additional scale below the diagram.

the evaporative supply of water vapor from the part of the sea surface directly below the column. However, the evaporation from a large area under the influence of a tropical cyclone is extremely important for supporting the convective activity in the central region of the cyclone. (This matter will be discussed further in Section 7.)

If the low-level convergence of convectively unstable air is to determine the distribution of organized convection, it is still necessary to introduce further hypotheses concerning the behavior of individual clouds in order to formulate the effects of convection. Although a great number of small cumuli are present in a tropical cyclone, their contribution to the energetics of the cyclone is probably very small. In terms of both precipitation and upward transport of heat and mass, tall convective clouds or "hot" towers around the cyclone center are the most important and dominant form of moist convection. The correspondence between the activity of "hot" towers and the convergence of the boundary layer inflow seems to be well supported by observational evidence (e.g., Riehl and Malkus, 1961). Therefore, within the present framework of the two-layer (plus boundary layer) representation, it is reasonable to assume that all convective clouds rise into the upper layer of the model contributing to the diabatic mass flux Q^+. More specifically, we may assume that Q^+ is given in the form

$$Q^+ = \begin{cases} \eta w, & \text{if } w > 0, \\ 0, & \text{if } w \leqslant 0, \end{cases} \tag{5.1}$$

where w has been defined as the vertical velocity at the top of the boundary layer and the nondimensional parameter η will be determined below from energy considerations.

Let us define H as the sum of the geopotential energy and the enthalpy (including latent heat) of a unit mass of moist air, i.e.,

$$H \cong c_p T + Lq + gz, \tag{5.2}$$

where c_p is the specific heat of air under constant pressure, T the temperature, L the latent heat of condensation, and q the mixing ratio of water vapor. In differential form, H may be expressed as

$$dH = (c_p T/\theta_e) d\theta_e. \tag{5.3}$$

Although unstable convective motions represent production of kinetic energy, the actual amount involved is negligible compared to other forms of energy considered in H. Time variations in the large-scale environment may also be neglected for the time scale of convective clouds, although the long-term effects of such variations should be considered for the time scale characteristic of cyclone development (see Section 6). Under these assumptions, we may consider H to be a conservative property of an individual parcel during a pseudo-adiabatic process. If two parcels of air with different values of H are mixed, the resulting H of the mixture may be given by the arithmetic average.

The parameter η introduced in (5.1) implies, for every unit mass of the boundary layer air that goes up in the convective cloud, that $(\eta-1)$ units of the air in the lower main layer are entrained into the updraft and, as a result, η units of the saturated cloud air enter the upper layer. If a representative value of H of the boundary layer air is denoted by H_0, that of the entrained air in the lower main layer by H_1, and that of the saturated mixture entering the upper layer in the updraft by H_2, the energy balance of the convective updraft is given by

$$\eta H_2 = H_0 + (\eta - 1) H_1,$$

or, after solving for η, by

$$\eta = 1 + \frac{H_0 - H_2}{H_2 - H_1}. \tag{5.4}$$

Since the range of relative variation of either H or θ_e is small, the factor in parentheses on the right-hand side of (5.3) may be considered to be a constant, and (5.4) may be expressed more conveniently in terms of θ_e. Let representative values of θ_e in the boundary layer and in the lower main layer be denoted by $(\theta_e)_0$ and $(\theta_e)_1$, respectively, and determined from the cyclone-scale distribution of θ_e. The quantity H_2 refers to the saturated cloud air in the upper layer, so that the corresponding equivalent potential temperature is not that of the ambient air, $(\theta_e)_2$, but rather, approximately, $(\theta_e^*)_2$. This is because the saturated cloud air should have substantially the same temperature as the environment in the upper layer. It may be noted that the last approximation does not contradict our recognition of "hot" towers. As was shown by Riehl and Malkus (1961), the relatively "hot" mass flux reaching near the tropopause is only a small fraction of the mass flux crossing the 500-mb level in the convective updraft.

In order to avoid excessive usage of subscripts and superscripts, we shall simplify the notation by introducing χ's defined by

$$\left.\begin{aligned} \chi_0 &= (\theta_e)_0 - \Theta \\ \chi_1 &= (\theta_e)_1 - \Theta \\ \chi_2 &= (\theta_e^*)_2 - \Theta \end{aligned}\right\}, \tag{5.5}$$

where Θ, an arbitrary constant, is introduced for convenience in numerical calculations and may be ignored in qualitative discussion. Then (5.4) may be written in the approximate form

$$\eta = 1 + \frac{\chi_0 - \chi_2}{\chi_2 - \chi_1}. \tag{5.6}$$

As will be discussed in the following sections, η is considered as a dependent variable because of possible variations in χ's.

The diabatic mass flux Q^- represents the effects of cooling processes. Several numerical experiments have been carried out with the present model under the assumption that the radiative cooling occurs uniformly over a large area. However, comparison of the corresponding cases with and without cooling showed little difference in the behavior of computed cyclones. Furthermore, even without cooling, no excessive warming of the whole system was found to occur, at least during the most interesting initial period of several days. Therefore, we shall discuss in this paper only the cases without cooling; that is,

$$Q^- = 0. \tag{5.7}$$

Although the differential cooling due to nonuniform cloud coverage may affect the development of a tropical cyclone, no attempt has been made to include such an effect in this study.

6. Effects of the warm core on convection

In the preceding section, the cumulus convection has been discussed as if there were no changes in the ambient atmosphere. Naturally, there should be compensating downward motion somewhere outside the updraft. If a substantial part of condensed water in the cloud should fall out of the atmosphere in precipitation, the downward motion may be assumed to be dry adiabatic and the adiabatic change of ambient temperature will accompany the vertical motion. However, since the atmosphere is stably stratified, the compensating downward motion does not occur in a horizontal

scale similar to that of convective clouds. As theoretical studies of convection in a conditionally unstable atmosphere indicate (e.g., Lilly, 1960), the stable downward motion is spread over an area which is not merely larger than the size of individual clouds, but which is, rather, even larger than a typical area of the inner convective region of a tropical cyclone.

In those circumstances, the increase of temperature in the convective region is not directly related to the amount of heat released in the same region. Instead, it depends largely on the cyclone-scale transverse circulation which produces adiabatic adjustments of the whole system in response to the moist convective activity near the center. Only a small fraction of heat energy released in moist convection is retained in the convective region—just so much as is necessary for adjusting the temperature and pressure to variations of the tangential circulation. The rest of the released energy is transmitted in the form of gravity waves to a wide outside area, even though the gravity waves do not explicitly appear under the balanced vortex approximation. Therefore, the ambient temperature variation may be considered to be part of the slow variation of the balanced vortex, as was discussed in Section 4, and it could be neglected in the preceding section where convective clouds were considered in their own time scale. However, in a much longer interval of time, the slow increase of temperature in a central region of the cyclone may become appreciable if the tangential circulation simultaneously increases in such a way as to support a large radial temperature gradient in the balanced state.

In the earlier study (Ooyama, 1964), the possible effect of temperature variations on moist convection was neglected, and the parameter η was fixed at a constant value derived from a standard distribution of equivalent potential temperature, such as that shown in Fig. 2. Although this model succeeded in producing development of a hurricane-like vortex, the assumption of constant η caused unchecked growth of the vortex. In the actual tropical cyclone, however, a considerable increase of temperature is observed near the center, particularly in the upper troposphere. Since the higher temperature in the upper layer requires more heat energy for the boundary layer air to rise to that layer in a convective updraft, the development of a warm core should cause reduction of the moist convective instability in that area. In order to incorporate this stabilizing effect in the variation of η, we now have to consider $(\theta_e^*)_2$, or χ_2 as defined by (5.5), as one of the dependent variables of the model.

In a balanced two-layer model, it is possible to take the potential temperature of each layer as a dependent variable, so that both the mean temperature of a vertical column and the static stability are explicitly predicted. Lorenz (1960) proposed a finite-differencing method for such a model, which would preserve both the average and the variance of potential temperature of a whole system under adiabatic processes. However, in the presence of intense heat sources, the computed static stability will depend very sensitively on the partition of heat sources between the two layers. Since the compatibility condition for balance in the two-layer model relates only the mean temperature to the motion field, the condition imposes almost no constraint on the diabatically caused change of the static stability. Therefore, if the computed stability is to have real significance, it is important that the diabatic heating be specified with sufficient accuracy, or at least, that the formulation of heating embody in itself some mechanism to regulate the computed stability. In the case of parametrized convection, this is not an easy requirement to fulfill on a firm physical basis. The usual practice in this regard is to adjust the vertical distribution of heat sources in such a way that the heating will, sooner or later, produce a moist adiabatic temperature profile. At the present level of knowledge of moist convection, this may be a reasonable procedure. However, it should be noted that such an assumption tends to overshadow the advantage in computing the static stability by Lorenz's two-temperature scheme.

In the present study we follow a simpler alternative by considering only the mean temperature of a vertical column as an intrinsic variable to specify the temperature structure of the two-layer model. The temperature of individual layers may, if necessary, be parametrically determined from the mean temperature by means of an assumed temperature profile. Actually, the temperature in the true thermodynamical sense is not defined in the present model, as was mentioned in Section 2. However, a certain model variable may be interpreted in terms of temperature.

Since the vertical shear of tangential motion is related to the radial temperature gradient under the balanced vortex hypothesis, it appears reasonable to define the mean potential temperature θ_m through the thermal wind equation for the gradient wind, i.e.,

$$c_p(\pi_1-\pi_2)\frac{\partial\theta_m}{\partial r}=\left(f+\frac{v_2}{r}\right)v_2-\left(f+\frac{v_1}{r}\right)v_1, \qquad (6.1)$$

where π_1 and π_2 are representative values of

$$\pi=(p/p_{00})^{2/7}$$

in the two main layers, and $p_{00}=1000$ mb. With the substitution of (3.1) and integration with respect to r from any radius to a sufficiently large radius, Eq. (6.1) becomes

$$\theta_m-\bar{\theta}_m=\frac{\phi_2-\phi_1}{c_p(\pi_1-\pi_2)}, \qquad (6.2)$$

where $\bar{\theta}_m$ is a standard value which θ_m is assumed to approach at large radius. By definition, ϕ_j vanishes at such radius.

In order to express the variation of θ_m in terms of χ_2, it is necessary to introduce an assumption on the vertical distribution of temperature. According to observations either in the core or in the outskirts of a tropical cyclone, the temperature profile in the middle and upper troposphere is very close to that of a moist adiabat. Suppose that θ_1 and θ_2 denote the representative potential temperatures of the lower and upper main layers, respectively, in a given column, and let us assume that θ_m is defined by the arithmetic mean of θ_1 and θ_2, and also that θ_1 and θ_2 lie on a moist adiabat. Then the equivalent potential temperature which marks the moist adiabat is uniquely determined as a function of θ_m. By definition, this equivalent potential temperature must be $(\theta_e^*)_2$ itself, which corresponds to the given θ_m. Note that no particular assumption is being made here concerning the general distribution of water vapor; the saturation has been assumed only inside the implicit convective clouds.

A typical range of variation of $(\theta_e^*)_2$ in a tropical cyclone is from 340 to 370K, which corresponds to the variation of θ_m from 324 to 339K if the representative pressures of the two main layers are taken to be 700 and 300 mb. Since the ranges of variation concerned are relatively small, we may simply adopt a linear interpolation formula

$$\chi_2-\bar{\chi}_2=2.0(\theta_m-\bar{\theta}_m). \tag{6.3}$$

Eliminating θ_m with (6.2), we obtain the desired equation for χ_2 in the form

$$\chi_2-\bar{\chi}_2=\alpha c_p^{-1}(\phi_2-\phi_1), \tag{6.4}$$

where α is a dimensionless constant factor of about 10.3 for the above choice of the representative pressures.

The choice of these pressures is arbitrary because it depends on the assumed height of penetrative convection. The numerical factor α could differ by as much as 15%, if an equally plausible but different choice were made. Furthermore, there is a degree of uncertainty concerning the optimum definition of the equivalent potential temperature. For example, one can argue whether or not the heat of fusion should be included. Although we shall not pursue the question further in the present paper, such a distinction could be very important if the purpose of numerical experiments were to investigate possible effects of cloud seeding on the behavior of a tropical cyclone.

7. The air-sea energy exchange

A vast amount of latent heat is already stored in the atmospheric boundary layer over the tropical ocean. If the moisture-rich air could be gathered and fed into convective clouds at a sufficient rate, the energetic requirement of a tropical cyclone might appear to be easily satisfied. However, since the effective area from which a tropical cyclone may collect the moist air cannot be infinitely wide, there is a question about the importance of the ocean directly under the influence of a tropical cyclone as a source of heat and moisture. Besides the amount of energy collected, there is the question of the quality of the moist air fed into convective clouds. If the equivalent potential temperature θ_e of the boundary layer remained constant, the moist convective instability around the center of the storm would soon decrease with development of a warm core. If the convection eventually becomes almost neutral, the mean temperature of the vertical column is not likely to increase much further, despite continued release of latent heat in the column.

Capitalizing on the fact that the eye wall of a tropical cyclone does not slope so much as was once believed, Malkus and Riehl (1960) showed that a central pressure much lower than 1000 mb would be difficult to explain hydrostatically if θ_e in the boundary layer were the same in the tropical cyclone as in the normal tropical atmosphere. According to their estimate, for example, θ_e must be 12.5K higher than normal in order to account for the surface pressure of 966 mb. Assuming a model hurricane with prescribed distributions of pressure and wind velocity in the boundary layer, they have further demonstrated that the air traveling in the layer from $r=90$ to 30 km can easily pick up enough heat and moisture to raise θ_e as required. However, the total amount of additional water evaporated from the ocean inside 90 km was found to be less than 10% of the amount of water vapor brought in by the inflow from outside. "Thus, curious enough," concluded the authors, "the oceanic source of water vapor, apparently so vital for the very existence of the storm, makes a negligible contribution to its water budget."

It seems to the present author that the paradoxical conclusion by Malkus and Riehl can be avoided if the evaporation from the ocean not only in the inner rain area but also in the outer area is taken into consideration. As we shall discuss below, the oceanic contribution of latent and sensible heat in the outer area may be of vital importance in fulfilling the total energetic requirement of a tropical cyclone, much as the additional contribution in the inner area is vital for maintenance of the low central pressure by furnishing the inflow air with an essential increment of equivalent potential temperature.

The frictionally induced inflow ψ_0 sharply decreases as it approaches the center, resulting in a rather abrupt lifting of the inflow air. This convergence of ψ_0 is responsible for the continued convective activity in the inner rain area, especially in the eye wall clouds. On the other hand, at a sufficiently large radius where the cyclonic circulation has not yet significantly developed, ψ_0 should have remained small, and should be still smaller at larger radii. Therefore, at any particular moment in the history of a tropical cyclone, ψ_0 must take a maximum value at some distance from the center, although the radius of maximum ψ_0 may change with time. Outside this radius, ψ_0 is divergent; the inward

increase of the inflow flux can be made up only by subsidence of the free atmospheric air into the boundary layer, with consequent decrease in θ_e of the boundary layer air due to dilution by mixing with the drier air from above. Therefore, the proportion of the original boundary layer air in the total ψ_0 reaching the inner convective region may become substantially reduced. Unless the heat and moisture supply from the ocean again raises θ_e to sufficiently high values before the inflow air reaches the inner region, either the convective activity will diminish or the supply of energy within the inner region must be much greater than the earlier estimate.

The subsidence at the top of the boundary layer may not be very large in terms of the vertical velocity, but it may be spread over a large area with a radius of a few hundred kilometers or more. With usually scarce observations of low-level winds and humidity in such an area, it is extremely difficult to obtain a reliable estimate of the total amount of water vapor supplied by the ocean under the influence of a tropical cyclone. Recently, however, interesting evidence on the importance of sea water evaporation has been obtained from tritium measurements by Östlund (1967). According to his analysis, 60–80% of the water in the eye wall of hurricane Betsy, 1965, could have evaporated from the ocean not so long ago. Even though the evidence is indirect, it clearly suggests that a tropical cyclone consumes a great deal more latent heat than it can collect from the pre-existing atmospheric vapor.

The usual practice in the formulation of air-sea energy exchange is to calculate the transfer of latent heat and sensible heat individually with semi-empirical formulas similar to those of Jacobs (1942). However, if we assume the same exchange coefficient for the two processes, the thermodynamical energy flux, comprising both latent and sensible heat, can be calculated by a single formula. Then the heat budget and the moisture budget of the boundary layer may be combined into a single equation in terms of H, which has been defined in Section 5 as the sum of the geopotential and enthalpy of moist air. That is, the thermodynamical energy equation for the boundary layer may be written in a conservation form,

$$\frac{\partial}{\partial t}(h_0 H_0)-\frac{\partial}{r\partial r}(\psi_0 H_0)+(w^+ H_0-w^- H_1) =C_E|v_1|(H_s-H_0), \quad (7.1)$$

where H_s is the value of H for saturated air at the sea surface temperature and pressure; w^+ and w^- are defined by

$$\left.\begin{aligned} w^+&=\tfrac{1}{2}(|w|+w)\\ w^-&=\tfrac{1}{2}(|w|-w)\end{aligned}\right\}, \quad (7.2)$$

so that both w^+ and w^- are zero or positive but only one of them may have a nonzero value equal to $|w|$, depending on the sign of w; and C_E is the nondimensional coefficient for the air-sea energy exchange. Since the actual variation of H in the lower tropical atmosphere is due mainly to the variation of water vapor mixing ratio, (7.1) may be considered to represent primarily the latent heat budget of the boundary layer.

Since the radial and vertical fluxes on the left-hand side of (7.1) depend on the drag coefficient C_D through (3.19), the relative magnitude of C_E to C_D may be expected to be one of the critical factors in determining the variation of H_0. Unfortunately, there is little information on C_E under hurricane conditions, other than the semispeculative guess that the exchange coefficients of latent heat, sensible heat and momentum are probably of the same magnitude. In the present study, we shall assume $C_E=C_D$ unless otherwise specified.

Under the same approximation as we have used in reducing (5.4) to (5.6), (7.1) may be written in terms of equivalent potential temperature or, for the sake of simpler notation, in terms of χ's. Let us add one more definition to (5.5), i.e.,

$$\chi_s=(\theta_e^*)_s-\Theta, \quad (7.3)$$

where $(\theta_e^*)_s$ is the equivalent potential temperature of the saturated air at the sea surface temperature and pressure. Then we may reduce (7.1) to

$$\frac{\partial \chi_0}{\partial t}+u_0\frac{\partial \chi_0}{\partial r}+\frac{w^-}{h_0}(\chi_0-\chi_1)=\frac{C_E|v_1|}{h_0}(\chi_s-\chi_0). \quad (7.4)$$

The sea surface temperature T_s will be assumed to be a prescribable parameter. On the other hand, the sea surface pressure p_s is a dependent variable determined from the first equation of (2.8) for $z=0$. Since the saturated equivalent potential temperature of the sea surface is a function of both p_s and T_s, we should consider χ_s to be a dependent variable, even if T_s is assumed to be constant. The variation of χ_s in the outer area, where a major part of the total evaporation may take place, is rather small, since the variation of p_s itself is relatively small there. However, a sharp decrease of p_s in the inner rain area can raise χ_s 10C or more in an intense tropical cyclone. This increase of χ_s may help the boundary layer inflow acquire additional moisture and heat in order to boost χ_0 shortly before the air ascends in the warm core. For this reason, we shall include the pressure dependency of χ_s in our model assuming a linear relation

$$\chi_s-\bar{\chi}_s=-\beta c_p^{-1}\phi_1, \quad (7.5)$$

where the dimensionless factor β, which can be determined from the definition of equivalent potential temperature, is about 1.87 for $T_s=28$C and $\bar{p}_s=1015$ mb; and $\bar{\chi}_s$ is the value of χ_s at $p_s=\bar{p}_s$ (that is, at $\phi_1=0$). Since the standard sea surface pressure $\bar{p}_s$ is fixed, $\bar{\chi}_s$ is a function of T_s. Their correspondence is shown in the

bottom part of Fig. 2 in terms of $(\theta_e^*)_s$, without involving the arbitrary constant Θ in (7.3) and (5.5).

In order to predict χ_0 with (7.4), it is necessary to know χ_1 at those radii where the subsidence ($w<0$) occurs. In the area of convective activity ($w>0$), the knowledge of χ_1 is also required for determining η from (5.6). Although it is relatively simple to formulate the variation of χ_1 due only to the temperature change, such variation does not amount to very much; a much larger variation of χ_1 may occur due to the possible variation of the mixing ratio in the lower main layer. In the case of χ_0, the prognostic equation has been written in a fairly simple form under the assumption that the eddy flux from the sea surface is the only major process to be considered besides the advective terms. If a prognostic equation for χ_1 is to be formulated, the eddy flux from the boundary layer is not necessarily the major source of water vapor for the layer concerned; evaporation of cloud droplets, including those of numerous non-precipitating small cumuli, may have to be taken into account. Furthermore, the fact that even over the ocean the tropical atmosphere is kept relatively dry (except in the lowest layer) suggests the importance of large-scale subsidence in the free atmosphere, which counteracts the upward transport of water vapor by moist convection and turbulence. These competing processes may occur in the tropical cyclone and, probably, in different proportions and magnitudes. At any rate, a realistic prediction of the mixing ratio in the free atmosphere appears to be an extremely delicate problem.

In order to keep the present model simple enough to be tractable, we shall assume χ_1 to be a prescribable model parameter. This is not to say that the variation of χ_1 is unimportant; it should be taken into consideration for further improvement of the model. Nevertheless, we may assume that a sophisticated treatment of χ_1 is probably not of critical importance for the understanding of the basic dynamics of a tropical cyclone. In order to explain the matter further, we may consider the general variation of χ_1 due to changes in the synoptic situation and the local variation of χ_1 within the cyclone, separately. With regard to the former, Simpson and Riehl (1958) and others have suggested that mid-tropospheric advection of air with low equivalent potential temperature affects the development of a hurricane. The "ventilation" effect may be simulated with the present model by artificially changing the prescribed value of χ_1. However, prediction of variations in the synoptic situation is beyond the scope of this study.

On the other hand, the local variation of χ_1 requires more careful consideration, especially in the region of the eye-wall clouds where the ambient air itself may become nearly saturated. Suppose that, due to the local increase of χ_1, $\chi_2-\chi_1$ happened to decrease to zero faster than $\chi_0-\chi_2$ did due to the upper warming. The value of η would then become infinite according to (5.6). However, if such a condition is ever approached in reality, the mid-tropospheric air of high humidity would be quickly used up in moist convection and replaced by less humid air, since the amount of humid air in the free atmosphere is limited and the rate of new supply of water is meager. Therefore, if the moisture budget in the free atmosphere is properly accounted for, the extreme condition in which the hypothesis behind (5.6) may break down is not likely to occur; or, if it does occur, the total amount of heat released under the breakdown condition is simply limited by the amount of moist air available, even if η were momentarily to become a theoretical infinity. It is much more probable in reality that $\chi_0-\chi_2$ becomes small faster than $\chi_2-\chi_1$ as a warm core develops with intensification of the cyclonic circulation. Then, in this limit, η approaches unity regardless of the exact value of χ_1, and Q^+ will be determined only by w; that is, by the supply of moist air due to the convergence of the boundary layer inflow. In this sense, the present assumption of neglecting the possible local variation of χ_1 by prescribing a constant value does not appear to be a grave simplification. On the other hand, if the apparent increase of χ_1 in the inner convective region were to be empirically prescribed without due consideration of the moisture budget, we might run the risk of introducing an unlimited source of latent heat into the mid-troposphere.

8. Linear analysis of the model

In view of the fact that only a few tropical disturbances actually grow into tropical cyclones, it is of practical importance, as well as of theoretical interest, to investigate the transformation of a weak, wavelike disturbance into an incipient cyclone. Variations of atmospheric and oceanic conditions in synoptic and sub-synoptic scales must have an intimate bearing on the fate of individual disturbances. Obviously, however, the present model with the axisymmetry assumption is not suitable for such investigations. All the numerical experiments in this study must begin by assuming the pre-existence of an axisymmetric disturbance. Furthermore, the physical and hydrodynamical processes formulated in this model may not be the dominant mechanisms among those governing weak disturbances. Therefore, while it is still possible to draw some inference from the numerical results as to what conditions are favorable (or unfavorable) for cyclonic development, application of the model to a very weak initial disturbance is limited in reality.

In spite of the limitation, however, it is still interesting to examine some dynamical characteristics of the model with the use of a linearized system of equations for small-amplitude perturbation. The linear analysis will be useful both in clarifying the *modus operandi* of the basic mechanism of tropical cyclone development and in providing some basis for comparison with later discussions of nonlinear results. For this purpose, we

shall assume in this section that ϕ_j, u_j, v_j, and their derivatives, including ζ_j, w and Q^+, are small perturbations superposed on the fluid system at rest and that their products are negligible. For the sake of simplicity, but without altering the essential character of the model (at least in the linear analysis), we may neglect the effects of curvature and treat the radius like the x axis of Cartesian coordinates. The axisymmetry, then, becomes equivalent to the assumption of no dependency on y.

In order not to eliminate the sea surface stress in the linearizing process, we shall temporarily replace (3.11) by

$$\tau_s=\rho k_s v_1, \tag{8.1}$$

where k_s corresponds to $C_D|v_1|$ in (3.11), but is here considered to a constant. Furthermore, in order to present the essence of linear analysis with a minimum of mathematical complexity, the conditional equation (5.7) is also temporarily replaced by the unconditional one

$$Q^+=\bar{\eta}w, \tag{8.2}$$

where $\bar{\eta}$ is a standard value of η determined from the undisturbed distribution of θ_e. The variation of η, which will prove to be crucial in nonlinear computation, does not appear in (8.2) because of linearization. If the internal friction were neglected, as has been done here, a pseudo-linear analysis could be made without assuming the unconditional "heating" (8.2), but with the conditional equation (5.1). However, as far as the growth rate of a disturbance is concerned, it matters little whether the region of $w<0$ is energetically passive ($Q^+=0$) or active ($Q^+<0$). Analyses with conditional heating have been given by Charney and Eliassen (1964) and Ogura (1964).

Under all the above assumptions with a minor addition of $h_1=h_2(\equiv\bar{h})$, we may obtain a complete set of linear perturbation equations in the following form:

The equations of continuity

$$\left.\begin{aligned}\frac{\partial}{\partial t}(\phi_1-\epsilon\phi_2)&=-\sigma g\left\{\bar{h}\frac{\partial u_1}{\partial r}+(\bar{\eta}-1)w\right\}\\ \frac{\partial}{\partial t}(\phi_2-\phi_1)&=-\sigma g\left\{\bar{h}\frac{\partial u_2}{\partial r}-\frac{\bar{\eta}}{\epsilon}w\right\}\end{aligned}\right\}, \tag{8.3}$$

$$h_0\frac{\partial u_0}{\partial r}+w=0. \tag{8.4}$$

The equations of tangential motion

$$\frac{\partial v_1}{\partial t}+fu_1=0,\quad \frac{\partial v_2}{\partial t}+fu_2=0, \tag{8.5}$$

$$fu_0+(k_s/h_0)v_1=0. \tag{8.6}$$

The geostrophic balance

$$fv_1=\frac{\partial\phi_1}{\partial r},\quad fv_2=\frac{\partial\phi_2}{\partial r}. \tag{8.7}$$

Eliminating all the variables except ϕ_1 and ϕ_2, we may reduce the above system of equations to the set

$$\left.\begin{aligned}\frac{\partial}{\partial t}(\phi_1-\epsilon\phi_2)&=2\bar{R}^2\frac{\partial^2}{\partial r^2}\left\{\frac{\partial\phi_1}{\partial t}-\frac{(\bar{\eta}-1)k_s}{\bar{h}}\phi_1\right\}\\ \frac{\partial}{\partial t}(\phi_2-\phi_1)&=2\bar{R}^2\frac{\partial^2}{\partial r^2}\left\{\frac{\partial\phi_2}{\partial t}+\frac{\bar{\eta}k_s}{\epsilon\bar{h}}\phi_1\right\}\end{aligned}\right\}, \tag{8.8}$$

where $\bar{R}$ has been defined by (4.6). The solution, which is symmetric at the origin, may be written in the form

$$\phi_j=\Phi_j e^{\gamma t}\cos(\pi r/2l), \tag{8.9}$$

where Φ_j is a constant, γ the growth rate and l the quarter wavelength. Since w has the same spatial distribution as (8.4), we may call l the radius of ascending region. The condition that (8.9) be nontrivial yields a characteristic equation, which is quadratic in terms of γ. One root, $\gamma=0$, is almost trivial since Φ_1 must vanish; that is, there is no disturbance in the lower layer and, thus, no convective activity. The other root of the characteristic equation is given by

$$\gamma=\frac{k_s(\bar{\eta}-1-\xi^2)}{\bar{h}(1+2\xi^2+\sigma\xi^4)}, \tag{8.10}$$

where the nondimensional scale parameter ξ is defined by

$$\xi^2=2l^2(\pi\bar{R})^{-2}. \tag{8.11}$$

One obvious conclusion of (8.10) is that $\bar{\eta}>1$ is a necessary condition for $\gamma>0$. In other words, unless the cloud-scale convection itself is unstable, the cyclone-scale disturbance will not grow. For disturbances of a very large horizontal scale, the inertial stability due to the earth's rotation becomes a dominant factor, so that the disturbance $\xi^2>\bar{\eta}-1$ will decay even if the convection is unstable. In a typical case with $\bar{R}=1000$ km and $\bar{\eta}=2$, the critical value of l for which γ becomes zero is about 900 km. Disturbances with a smaller radius of ascending region may grow exponentially with time—the smaller the disturbance, the faster it grows. However, for disturbances with $l\lesssim 300$ km (that is, $\xi^2\ll 1$), the growth rate γ becomes practically independent of l.

The growth rate for much smaller disturbances can be expected to fall off if internal friction is included in (8.5). Such an analysis has actually been made and its results are shown in Fig. 3. The adopted values of some key parameters are $\bar{h}=5$ km, $k_s=1.5\times10^{-2}$ m sec^{-1} (corresponding to $C_D=1.5\times10^{-3}$ and $v_1=10$ m sec^{-1}), and $\lambda=10^3$ m^2 sec^{-1}. The value of $\bar{\eta}$ is indicated in the figure. In the typical case of $\bar{\eta}=2.0$, the maximum

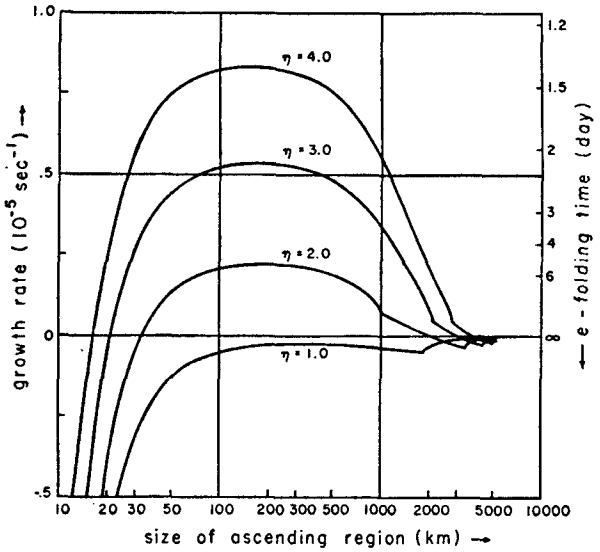

FIG. 3. The growth rate of small-amplitude disturbances as a function of the horizontal scale l (size of ascending region).

growth rate of 2.45×10^{-6} sec^{-1} (the e-folding time of about 5 days) occurs near $l=200$ km, although the growth rate is nearly constant between $l=50$ and 500 km. When compared to the e-folding time of about one day, which has been observed with tropical cyclones in a rapidly intensifying stage, the above figure for the growth rate seems to be a little small. However, since $\gamma \propto k_s$ according to (8.10), and nearly so even in the case with internal friction, the differences between the theoretical value and the observed extreme value of γ is reconcilable if one takes into account the fact that the adopted value for k_s is much too small to be representative of intensifying cyclones. Of course, a larger value of $\bar{\eta}$ than the assumed one can also contribute to faster growth.

Within the validity of linearization, the basic mechanism of the tropical cyclone development may be explained as follows. If a weak cyclonic vortex is initially given, there will be organized convective activity in the region where the frictionally induced inflow converges. The differential heating due to the organized convection introduces changes in the pressure field, which generate a slow transverse circulation in the free atmosphere in order to re-establish the balance between the pressure and motion fields. If the equivalent potential temperature of the boundary layer is sufficiently high for the moist convection to be unstable ($\eta>1$), the transverse circulation in the lower layer will bring in more absolute angular momentum than is lost to the sea by surface friction. Then the resulting increase of cyclonic circulation in the lower layer and the corresponding reduction of the central pressure will cause the boundary layer inflow to increase; thus, more intense convective activity will follow. As long as η remains greater than unity, this positive feedback process between the cyclonic circulation and the organized convention will continue.

It is true that the linearized model fails to account for many prominent features of real tropical cyclones. For example, the maximum w at the center, rather than at some distance from the center, fails to explain the eye formation. However, this failure is due to the omission of centrifugal acceleration for the sake of linearization. The upper layer circulation near the center should become cyclonic, rather than anticyclonic as the perturbation solution implies; the discrepancy is due to the omission of vertical transport of angular momentum in the linear analysis. The fact that most tropical disturbances do not grow into intense cyclones may be explained, at least partially, by the rather small growth rate of weak disturbances; adverse influences which are not included in this model may have a greater chance to interfere with the positive feedback process while a cyclone is weak than after it has grown into a well-organized intense storm. On the other hand, the fact that all tropical cyclones eventually stop intensifying must be explained by taking into account the reduction of η due to the establishment of the warm core.

The area of active convection in a tropical cyclone rarely extends beyond 100 km from the center; it is often much smaller in an immature, but intensifying, cyclone. However, the growth rate analysis with the linear model does not account for nature's preference for a relatively small convective area. According to the results shown in Fig. 3, a disturbance with $l=500$ km may grow just as fast as another with $l=50$ km. This shortcoming of the linear analysis is due neither to the peculiar assumption of an unconditional heat source (8.2), nor to the use of Cartesian geometry. Without employing these approximate procedures, Charney and Eliassen (1964) and Ogura (1964) obtained results almost identical to (8.10) from a growth rate analysis analysis for the case of no internal friction. Essentially similar results in this regard have also been obtained from the linear analysis of a primitive-equation model by Syōno and Yamasaki (1966).

In the absence of a satisfactory explanation by linear models, it is reasonable to assume that the size of the convective area in observed tropical cyclones is controlled by nonlinear mechanisms. However, no specific suggestions as to possible mechanisms can be found in the literature, except for kinematic arguments based on steady-state cyclone models (Kuo, 1959; Riehl, 1963).

One possible control mechanism that seems to be significant in the present model is the radial variation of equivalent potential temperature in the boundary layer. As was discussed in Section 7, χ_0 outside the convective area may be reduced by subsidence of drier air from the free atmosphere. Then, even though evaporation from the ocean is always working to increase χ_0, the air in the boundary layer will have to travel some distance inward before it regains a sufficiently high value of χ_0 to participate in active convec-

tion. Therefore, the area of moist convection cannot arbitrarily expand. It is even possible for the area to shrink under such circumstances. The importance of this fact that the rate of oceanic energy supply is finite, although it may be variable, will become evident when numerical results with the present model are discussed.

Although subsidence does play a significant role in limiting the area of moist convection in the model, and probably in nature as well, there are indications that it alone is not sufficient to explain the relatively small convective area found in real tropical cyclones. The possibility of other controlling mechanisms will be discussed in Section 15.

9. Specification of numerical experiments

With the model described above, a large number of numerical experiments have been carried out for various combinations of parameters and initial conditions. As it is neither possible nor necessary to present all the results in this paper, we shall first study a typical case in detail, and then examine only some special aspects of interest for several other cases.

The model parameters chosen for the typical case (called Case A) are listed in Table 1. The symbols in the first column of the table have been defined in the sections indicated in the second column. A few remarks on the assumed values may be briefly given: 1) The arbitrary constant Θ has been chosen to be equal to a standard value of $(\theta_e^*)_2$ (see Fig. 2) so that $\bar{\chi}_2=0$ by definition. 2) The given value of $\bar{\chi}_s$ corresponds to the sea surface temperature, $T_s=27.5$C. 3) The given value of f corresponds to the latitude 20N. 4) The coefficient μ for the shear stress at the interface corresponds to the vertical Austausch coefficient of about 2.5 m^2 sec^{-1}. It may be noted that the vertical transport of angular momentum due to convective clouds is not included in the eddy transport represented by μ, but is separately accounted for in (3.16). 5) If Richardson's empirical formula [see, e.g., Taylor (1959)] is applied, the given value of the lateral eddy-viscosity coefficients, λ_1 and λ_2, corresponds to an effective eddy size of about 6 km, which is a reasonable value in the vicinity of the eye-wall clouds, where lateral friction makes an important contribution to the angular momentum budget. 6) It is not necessary to give the fluid density an explicit value in order to integrate the model. However, in order to interpret ϕ_1 in terms of the sea surface pressure, we may assume $\rho=10^{-3}$ gm cm^{-3}.

The drag coefficient C_D for the sea surface stress is one of the most critical parameters of the model. However, as was summarized by Roll (1965), empirical determination of the coefficient is a problem that is still far from settled. As one likely possibility in this rather uncertain situation, it is assumed that C_D increases linearly with the wind speed and is given by

$$C_D=(0.5+0.06v_1)\times10^{-3}, \tag{9.1}$$

where v_1 is measured in m sec^{-1}.

TABLE 1. Specifications of Case A.

Symbol	Section where defined	Assumed value
ϵ, σ	2	0.9, 0.1
h_0	2	1 km
$\bar{h}_1$, $\bar{h}_2$	2	5 km
g	2	9.8 m sec^{-2}
f	3	5×10^{-5} sec^{-1}
r_x	4	10^3 km
R	4	10^3 km
Θ	5	342K
$\bar{\chi}_s$	7	30K
$\bar{\chi}_0$	5, 7	10K
χ_1	5, 7	-10K
$\bar{\chi}_2$	5, 6	0K
α	6	10.0
β	7	2.0
λ_1, λ_2	5	10^3 m^2 sec^{-1}
μ	5	5×10^{-4} m sec^{-1}
C_D	3, 9	variable: Eq. (9.1)
C_E	7	$=C_D$
$\hat{v}$	9	10 m sec^{-1}
$\hat{r}$	9	50 km
$\hat{\eta}$	9	2.0

As defined in (3.11), C_D is the coefficient for τ_s in terms of the gradient wind. However, the drag coefficient is usually defined in the literature in terms of wind speed near the surface, and it should be somehow converted to the same definition so that a comparison may be made with (9.1). For example, if the wind speed at the 10-m level can be assumed to be 80% of the gradient wind, a linear relation suggested by Sheppard (1958) for the 10-m level drag coefficient over the sea surface becomes

$$C_D=(0.51+0.058v_1)\times10^{-3}.$$

This is almost identical to (9.1), although there is some question as to the extension of Sheppard's formula to very high winds. Palmén and Riehl (1957) and Miller (1958a, 1963) have made estimates of C_D under hurricane conditions by applying angular momentum considerations to low level wind data. According to Miller (1963), these estimates seem to support a linear increase of C_D with wind speeds up to 50 m sec^{-1} or higher; his linear regression line may be expressed by the formula

$$C_D=(0.7+0.07v)\times10^{-3},$$

where v is a representative wind speed in the frictional inflow layer. This is again very similar to (9.1). Of course, there are other empirical estimates of C_D which do not necessarily support the linear dependency on wind speed. For the purpose of comparison, numerical experiments have also been made with the assumption of constant C_D.

All model parameters having been specified, the complete state of the model cyclone at any given time can be determined from the radial distributions of ϕ_1, ϕ_2 and χ_0. These three fields are the primary variables which are actually predicted in time integration of the models; concurrent distributions of all the other

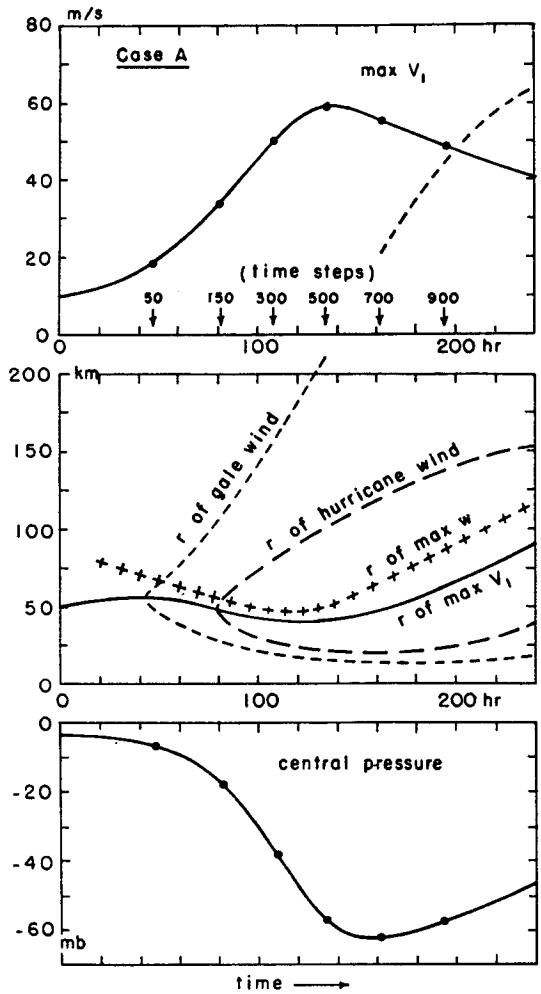

FIG. 4. Development of computed tropical cyclone in Case A: top, max v_1; middle, radii of max v_1, and max w, and outer and inner limits of hurricane- and gale-force winds; bottom, central surface pressure expressed as deviation from the normal. (The curve for the gale-wind limit extends into the top diagram.) Dots on curves indicate the time points selected for detailed illustration in Figs. 5 and 6.

variables are determined through diagnostic equations. However, we may specify the initial conditions for a numerical experiment in terms of v_1, v_2 and η, which can easily be converted to the conditions in terms of ϕ_1, ϕ_2 and χ_0. In all the numerical experiments reported in this paper, the initial conditions at $t=0$ are given in the form

$$v_1=\hat{v}\frac{2(r/\hat{r})}{1+(r/\hat{r})^2}, \tag{9.2}$$

$$v_2=0, \tag{9.3}$$

$$\eta=\hat{\eta}, \tag{9.4}$$

where $\hat{v}$, $\hat{r}$ and $\hat{\eta}$ are constant parameters to be specified. The assumed values for Case A are listed in Table 1. It may be noted that $\hat{v}$ is the maximum tangential wind in the lower layer, and $\hat{r}$ the corresponding radius. The upper layer is initially at rest.

Specification of the numerical experiments is not complete without a description of the computational procedures. However, since the model equations already incorporate the discretization in the vertical, the finite difference approximations for radial and time derivatives are largely a matter of computational technique, details of which may be found in the Appendix. Only a few basic facts are given here. The radial increment Δr is chosen to be 5 km, so that the radial axis from 0 to 1000 km is covered by 200 equal intervals. The time increment Δt is not fixed at a constant value, but is programmed to vary automatically during computation so that a certain condition for computational stability is always satisfied without making use of unnecessarily small Δt. In Case A, for example, Δt is 1 hr at the start of integration; it is gradually reduced to 0.12 hr as the computed cyclone intensifies and then increased to 0.24 hr by the end of a 10-day integration period; the total number of computational time steps is 1100. The required computation time on a CDC 6600 computer at the Courant Institute of Mathematical Sciences, New York University, is about 7 min.

The exact specification of numerical experiments other than Case A are given in the following sections. However, for convenience of reference, the main features of these experiments are outlined below.

Case B: The sea surface temperature T_s is about 2C lower than in Case A.

Case BA, AB: T_s is raised or lowered in the course of integration.

Case C_1, C_2, etc.: T_s is the same as in Case A only inside a certain radius, but is colder outside.

Case D: Both C_D and C_E are constant (independent of wind speed).

Case E_1, E_2: No energy supply from the ocean is assumed ($C_E=0$).

Case AE: The oceanic energy supply is stopped after the Case A cyclone has attained maximum intensity.

Case Ai_1, Ai_2, etc.: Initial conditions are different from those of Case A.

Case Afi_1: Very small eddy viscosity is assumed.

10. Typical results of numerical integration

The intensity of a tropical cyclone is usually measured in terms of either the minimum surface pressure or the maximum wind speed. In order to indicate the horizontal extent of the storm, the maximum radius of either hurricane- (64 kt) or gale-force (34 kt) winds may be referred to as the size of the cyclone. The radius of the maximum wind is also sometimes considered to be an indicator of storm size. Size and intensity alone are, of course, inadequate for describing structural details.

but they are convenient for the purpose of characterizing the time variation of a computed cyclone in compact form. The results of numerical integration in Case A are summarized first in terms of these simple parameters.

As shown in Fig. 4 (top), the maximum tangential wind, max v_1, increases from 10 to 58 m sec^{-1} in about $5\frac{1}{2}$ days (134 hr), despite a rather small rate of increase during the first two days. After attaining the peak, the maximum wind slowly decreases. However, this decrease should not be construed as a weakening of the cyclone as a whole; on the contrary, as shown in Fig. 4 (middle), the outer limits of both hurricane- and gale-force winds are still expanding even at the end of the 10-day integration period. The decrease of the central pressure shown in Fig. 4 (bottom) is very slow during the first few days but becomes faster as the wind speed increases. By the time max v_1 attains its peak, the central pressure is already 58 mb below normal. However, the lowest pressure of 63 mb below normal (that is, 952 mb if $\bar{p}_s=1015$ mb) is reached about one day later. Another interesting feature shown in Fig. 4 is the time variation of the radius at which max v_1 occurs. This radius increases slightly during the first two days when the cyclone is still weak, starts to decrease as soon as the rapid intensification sets in, and then increases again after the intensification ceases. The reversal of tendency at about the time of peak intensity is also seen in the time variation of the radius of the maximum vertical velocity, max w.

It is difficult to verify the results shown in Fig. 4 against the observed behavior of a tropical cyclone. The life history of tropical cyclones is extremely diverse and no single storm may behave exactly like an average one. However, among those tropical cyclones that remain over warm tropical waters for a long period, there is a certain pattern of evolution that may be considered to be a typical life cycle (Dunn, 1951; Riehl, 1954). If this typical life cycle, which is customarily divided into four stages, is compared with that of the simulated cyclone, a striking similarity appears between them.

1) The incipient (or formative) stage. Here a tropical disturbance is transformed into an organized but weak vortex. The development in this stage is usually a slow process; it may take several days for the surface pressure to drop to about 1000 mb. As was discussed in Section 8, the present model is not capable of simulating the transformation of a wave disturbance into a vortex. However, as far as the simulated cyclone in Case A is concerned, the initial period of 50–60 hr in which the intensification occurs very slowly may be considered as part of the incipient stage. The duration of this stage of a computed cyclone depends on the choice of initial conditions. Other numerical cases which begin with a weaker initial vortex than that in Case A will be presented in Section 15.

2) The deepening (or immature) stage. The incipient cyclone rapidly develops into a full-fledged hurricane or typhoon. It is not unusual in nature for the surface pressure at the center to deepen 20–30 mb in a 24-hr period, while the area of hurricane-force winds is confined to a relatively narrow band around the center. In Case A, the period approximately from $t=60$–130 hr represents the deepening stage.

3) The mature stage. In this stage, the intensity in terms of either maximum wind speed or central pressure surface reaches a limit and may gradually become less intense. However, this stage is marked by further outward expansion of the surface isobars and the stormy area. Therefore, the size of mature tropical cyclones may vary considerably. This stage may last for several days if the cyclone does not move out of the warm ocean. In Case A, the integration period beyond $t=130$ hr may be called the mature stage.

4) The decaying stage. Very rarely does a fully developed tropical cyclone dissipate over the warm tropical ocean. A tropical cyclone may dissipate, or transform into an extratropical cyclone when it moves onto a continental land mass, or when it enters colder northern waters. This final stage of a tropical cyclone may begin at any time, or even prior to, the mature stage. On the other hand, the tropical oceans are apparently not large enough to allow the cyclone to die a natural death. Therefore, although the numerical integration in Case A could have been continued beyond 10 days, results of such an experiment would not represent the fate of real tropical cyclones. In order to simulate the decaying stage in a more realistic manner, a certain model parameter such as the sea surface temperature or the coefficient of evaporation may be externally modified during the course of integration. Results of such experiments are discussed in Sections 13 and 14.

Now that the gross characteristics of the computed cyclone have been demonstrated, we proceed to examine the internal structure in detail. Figs. 5 and 6 show the radial distributions from the center to 400 km of various variables at six selected points in time. The time intervals between adjacent columns are approximately 30 hr; the position of each selected time relative to the life cycle is indicated by a dot on the curves in Fig. 4.

The first row of both Figs. 5 and 6 shows radial distributions of v_1, v_2 and $-u_0$. Development of v_1 with a sharp maximum until 134 hr and a subsequent broadening of the maximum during the mature stage are clearly shown. The outside flank of the v_1 profile, up to 400 km or so, fits very well a distribution of the form $v_1=\text{const}\times r^{-n}$, with $n=0.8$ during the deepening stage; during the mature stage, n decreases gradually to about 0.7.

In the upper layer, where the radial flow is outward, the tangential circulation should generally become anticyclonic ($v_2<0$). However, in an area around the center where the cyclonic angular momentum is transported from the lower layer by the diabatic mass flux, v_2 actually becomes cyclonic and increases as v_1 increases.

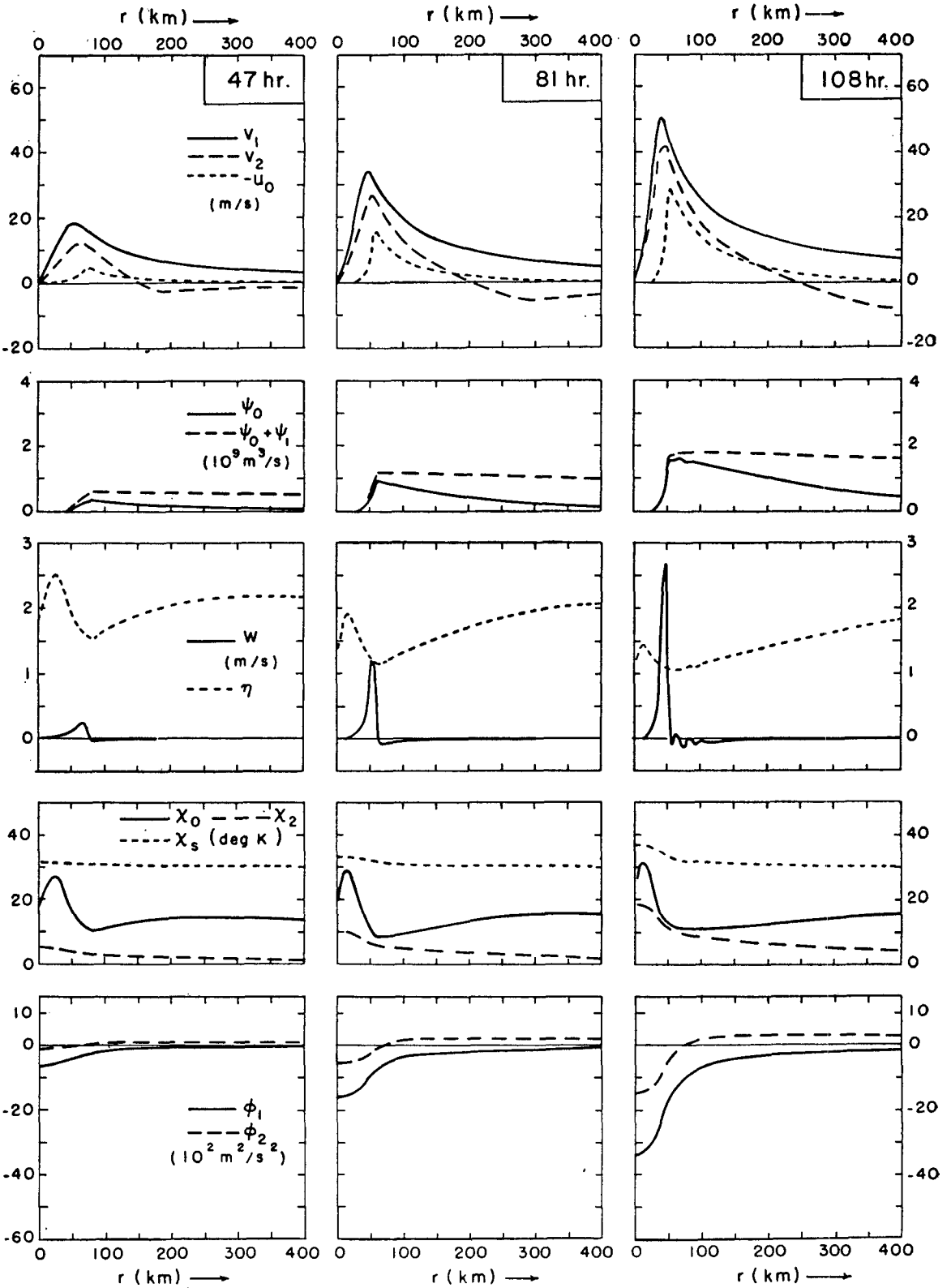

FIG. 5. Radial distribution of various field variables from 0 to 400 km in Case A at t=47, 81 and 108 hr.

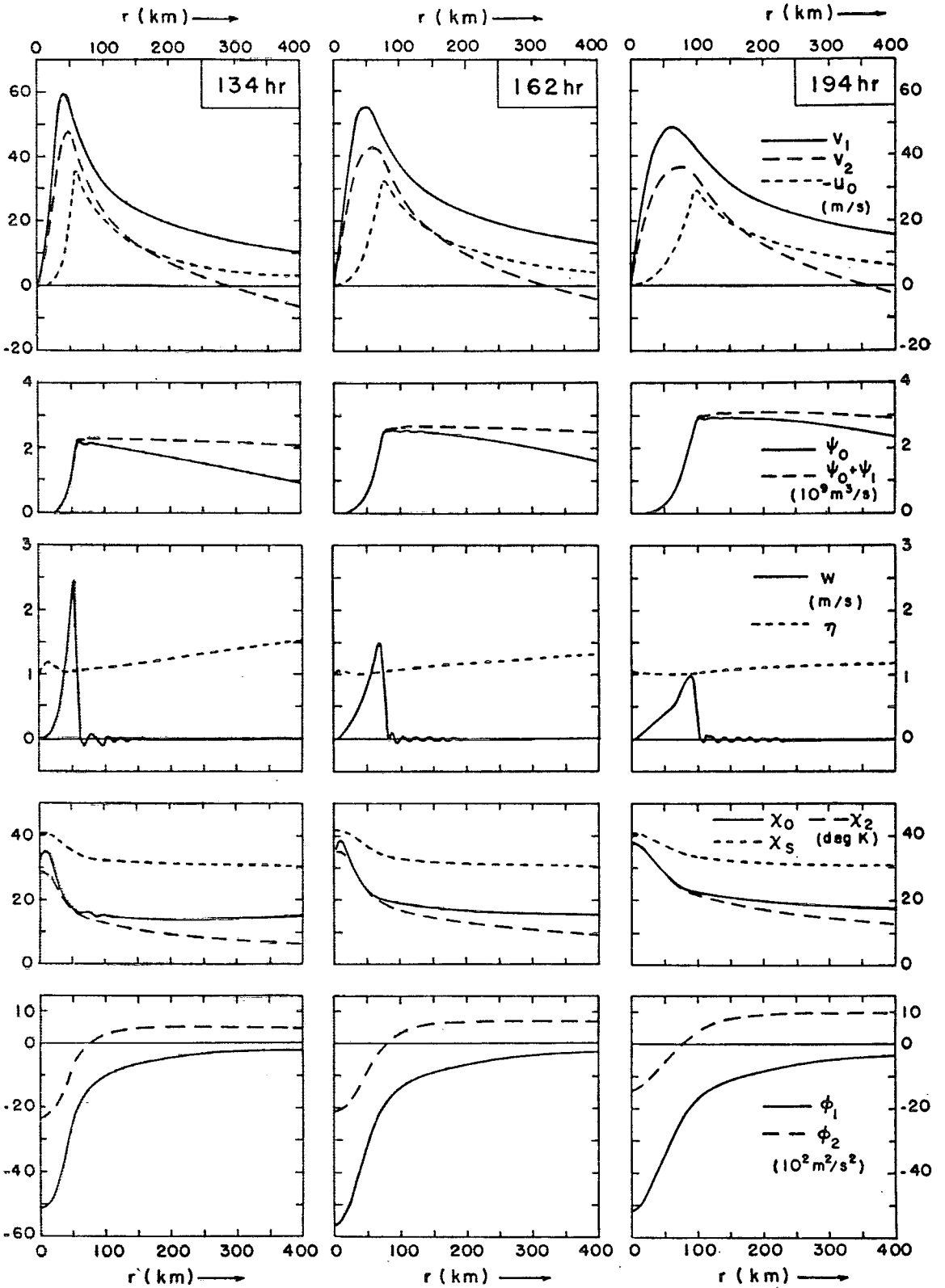

FIG. 6. Radial distribution of various field variables from 0 to 400 km in Case A at $t=134$, 162 and 194 hr.

The area of this upper cyclonic circulation expands with time, but the rate of expansion is less than half of u_2 at the edge. In the anticyclonic outer region, v_2 reaches a minimum value (negative maximum) as is shown on the v_2 curves at 47 or 81 hr. At other times the minimum v_2 is off the scale of the diagrams. Thus, for example, min $v_2 = -9.5$ m sec^{-1} at $r = 460$ km at $t = 134$ hr, and -13.7 m sec^{-1} at 640 km at 194 hr. It should be noted that the absolute vorticity, $f+\zeta_2$, becomes negative in a certain radial interval where v_2 rapidly decreases with r. For example, at 134 hr, $f+\zeta_2$ is negative with an average value of -1.86×10^{-5} sec^{-1} in the interval from $r = 60$ to 450 km. At other times the radial interval is different but the negative magnitude is about the same or less. Implications of the negative absolute vorticity in the upper layer have been discussed in Section 4. It may be added here that the reason for the negative absolute vorticity is the injection of heigher and higher cyclonic angular momentum from the lower layer into the upper central region, replacing outgoing fluid of lower angular momentum. Therefore, the appearance of negative absolute vorticity in the model cyclone is not a cause, but merely a consequence of the tropical cyclone development.

Since $v_0 = v_1$ in the present model, the inflow angle of the boundary layer inflow may be determined from the ratio of $-u_0$ to v_1. A maximum inflow angle of 36° occurs at 60 km shortly before 134 hr. The divergence or convergence of the boundary layer inflow is more clearly seen from the radial distribution of ψ_0 in the second row of Figs. 5 and 6, and also from the distribution of w in the third row. It may be noted, as w depends on the third-order derivative of the pressure field, that the computational noise is most conspicuously shown on the curves of w. (The dominant scale of the noise is about $4\Delta r$.) Despite the noise, however, the two major aspects in the radial distribution of ψ_0, or w, are evident. One is the sharp maximum of w, or the sudden convergence of ψ_0 near the radius of max v_1, which may be identified with the cause of eye-wall convection. Dynamically, this is due to the fact that further penetration of the inflow into the core of the vortex is resisted by the strong inertial stability in the core when the tangential circulation is almost like a solid rotation; for example, at 134 hr, the mean absolute vorticity inside 40 km radius is 233×10^{-5} sec^{-1}, compared with 22×10^{-5} sec^{-1} at 60 km or 13×10^{-5} sec^{-1} at 100 km. The other notable aspect is the weak but widespread subsidence into the boundary layer in the outer area. This feature may be difficult to see from the curves of w, since the magnitude of negative w is generally 3 cm sec^{-1} or less, except for computational irregularities. However, in terms of the total mass entering from the lower main layer to the boundary layer, the general subsidence is clearly seen from the gradual increase of ψ_0 with decreasing radius.

The total inflow flux, $\psi_0+\psi_1$, is also shown on the second row of Figs. 5 and 6. Since the outflow ψ_2 in the upper layer, does not exactly cancel the inflow, the surface pressure varies with time. However, the net mass flux, $\psi_0+\psi_1+\psi_2$, at any radius is found to be at least two orders of magnitude smaller than either the total inflow or the outflow. If $-\psi_2$ were plotted on the diagrams, it would be indistinguishable from the curve of $\psi_0+\psi_1$. The very slow variation of the total inflow flux, as well as that of the outflow flux, is due to the fact that the inertial stability in the outer area is very small in comparison with the static stability; the radial variation of those fluxes becomes appreciable only if it is examined over a radial distance comparable to the Rossby radius of internal deformation (about 1000 km). In terms of the velocity, the radial motion in the main layers is rather small; the overall maximum value of u_2 is 6.3 m sec^{-1} at 55 km at about 134 hr, and $-u_1$ has never exceeded 1 m sec^{-1} at any radius during the period of integration.

For the purpose of understanding the transition from the deepening stage to the mature stage, the most revealing information comes from the radial and time variations of the thermodynamic variables—η in the third row, and χ_0, χ_2 and χ_s in the fourth row of Figs. 5 and 6. [Note that although w(m sec^{-1}) and η are shown on the same numerical scale, the latter is a dimensionless variable.] As has been mentioned in Section 9, $\eta = 2$ has been assumed initially. However, already at 47 hr, η deviates considerably from the initial value within 200 km, reflecting changes mainly in the distribution of χ_0. The fact that χ_0 remains smaller than χ_s indicates that the sea surface is always supplying sensible and latent heat to the boundary layer inflow. However, during the deepening state (until 134 hr), a significant increase of χ_0 is found only inside the vortex core, where a negligibly small inflow occurs. In the other area, χ_0 remains almost unchanged or even decreases during this period due either to subsidence of the drier air into the boundary layer or inward advection of lowered χ_0. The rate of energy transfer from the sea surface increases as the vortex intensifies, but so does the subsidence due to divergence of ψ_0. Consequently, the minimum of χ_0 is maintained at the outer edge of the eye-wall convection and its position tends to shift inward. In accordance with the qualitative discussion at the end of Section 8, these computational results may explain why the convective activity is confined to a small area during the deepening stage.

While the distribution of χ_0 remains nearly stationary, the upper layer temperature represented by χ_2 steadily rises, particularly in the central area, as the cyclone intensifies. As is shown in the diagrams of η and w, the result of the warm core development is the decrease of convective instability in the very area where moist convection is actually taking place. At about 134 hr, the curve of χ_2 finally touches that of χ_0; that is, η is reduced to unity in the vicinity of max w. Now that the moist convection has become almost neutral,

further intensification of max v_1 stops, although a little more deepening of the central pressure continues until about 162 hr. By this time, the moist stability in the inner region is almost completely neutral. Since the peak intensity in terms of max v_1 and the lowest central pressure at the surface are not reached at the same time, it is difficult to define a single moment of time as the transition point from the deepening or immature stage to the mature stage. However, the physical nature of the transition is clearly characterized by neutralization of the eye-wall convection.

The intensification of the cyclone having come to an end, the divergence of ψ_0 outside the convective region becomes weakened, as is shown by the flattening of the ψ_0 curves outside the maximum. Then, with little competition from subsidence of the drier air, the evaporation works to increase χ_0 in a wider area then before, resulting in the gradual expansion of the convective region. Near the outer edge of this convective region, η remains slightly greater than unity. This much convective instability is apparently enough to increase the total kinetic energy of the cyclone during the mature stage.

The pressure dependency of χ_s, which was discussed in Section 7, is shown in the diagrams as the upward bulge of the χ_s curves. It is certain that the simulated cyclone in Case A could not attain the full intensity as shown if there were no increase of χ_s due to the pressure effect. However, this effect does not seem to be of crucial importance for development of a tropical cyclone. In a numerical experiment, in which all the specifications except $\beta=0$ are identical to Case A, the computed cyclone has attained a maximum intensity of 51 m sec^{-1} and 970 mb.

The last row of Figs. 5 and 6 shows the pressure field in terms of ϕ_1 and ϕ_2. The development of a sharp low pressure area during the deepening stage and the broadening of the low pressure area during the mature stage are evident. In the upper layer, the pressure generally rises above the normal value except in the small central area so that a broad high pressure ring is created around the central low. Although it is hard to recognize on the diagrams, ϕ_2 decreases with the radius in the outer area where $v_2<0$. No difficulty has been experienced in computing the gradient wind in the anticyclonic region.

11. Energy equations

The tropical cyclone, like other weather systems, may be considered to be a thermodynamic engine which generates kinetic energy from heat. However, the tropical cyclone differs from the extratropical variety in the sense that the former depends entirely on the latent heat released in a small inner region, while the latent heat in the latter is rather a supplementary source of energy. The observational study of the energetics is not an easy one; diligence and ingenuity are often called for in order to complement insufficient data. Nevertheless, Palmén and Riehl (1957) and others have made important contributions to our present knowledge of the tropical cyclone energetics. It will be interesting to compare the energy budget of the simulated cyclone with that of the observed.

The forms of energy we shall explicitly consider with the present model are the kinetic energy K_1 in the lower layer, the kinetic energy K_2 in the upper layer, and the potential energy P. Since activities within the cyclone are spatially nonuniform, it will be interesting to calculate the energy budget not just for the total area covered by the model but, rather, for the several subdomains separately. Therefore, we define, K_1, K_2 and P as the amount of energy over any given radial interval (r,r'); that is,

$$K_1=\int_r^{r'}\frac{1}{2}h_1v_1^2rdr, \tag{11.1}$$

$$K_2=\int_r^{r'}\frac{\epsilon}{2}h_2v_2^2rdr, \tag{11.2}$$

$$P=\int_r^{r'}\frac{g}{2}\{\sigma h_1^2+\epsilon(h_1+h_2)^2\}rdr. \tag{11.3}$$

Each integral in these definitions should have been multiplied by a constant factor $2\pi\rho$. However, since ρ is an arbitrary constant in this model, the factor has been omitted from the above as well as from definitions (11.9)–(11.18).

Under the hydrostatic and axisymmetric balance assumption, the kinetic energy due to vertical and radial components of motion is not included in (11.1) and (11.2), although these components play important roles in conversion and transport of energy. Similarly, due to the use of diagnostic equations, the amount of kinetic energy in the boundary layer becomes irrelevant to the energy budget, although the energy conversion and transport by the boundary layer inflow make important contributions to the energy budget of the main layers.

One significant difference between the energetics of the present model and that of real tropical cyclones is the lack of internal energy in the model due to the use of an incompressible fluid system. Although the use of the artificial system has proved to be no great hindrance in this study, a certain adjustment is needed in the interpretation of the energy budget in order to compensate for the missing internal energy. This problem will be discussed in the next section when we estimate the amount of rainfall in the simulated cyclone.

A complete account of the energy budget in an open subdomain is fairly complicated since energy is not only converted from one form to another within the subdomain but transported from or to neighboring domains in various forms. In order to simplify our discussion, the

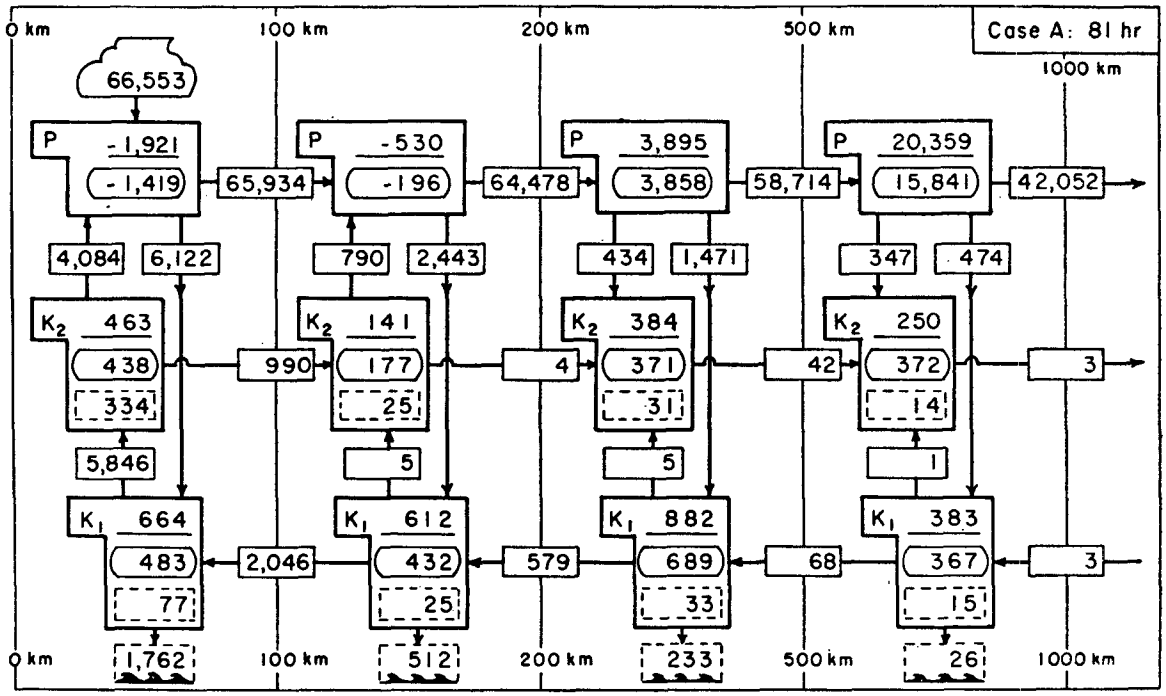

FIG. 7. Energy budget of the computed tropical cyclone in Case A at $t=81$ hr (deepening stage). The budget is calculated for four annular rings separately to show interdependency among different parts of the cyclone. Underlined values indicate the amount of energy of each kind (in units of 6.28×10^{13} joules), while the values in ovals represent the rate of energy change, and the values in dashed rectangles the rate of energy dissipation. The numbers in the cloud-shaped figures indicate the rate of diabatic energy input, while those in the solid rectangles show the rate of conversion or transport (in units of 6.28×10^{8} joules sec^{-1}).

following notation will be adopted: Let E or E' represent any one of K_1, K_2 or P. Then, the rate of change of E in the interval (r,r') is denoted by $[E]$, that is

$$[E]=\frac{\partial}{\partial t}E. \tag{11.4}$$

The rate of conversion of energy from E to E' within the interval is denoted by $[E,E']$. The inward flux of energy in the form of E across the circular boundary at radius r is denoted by $\langle E]_r$, and the outward flux by $[E\rangle_r$. Since the positive direction of conversion or transport is a matter of convenience, we may write

$$\left.\begin{aligned}[E,E']&=-[E',E]\\ \langle E]_r&=-[E\rangle_r\end{aligned}\right\}. \tag{11.5}$$

A special case in the above notation is $[K_1,K_2]$, which may be called the vertical transport of kinetic energy rather than the conversion of K_1 to K_2. As an extension of the above notation, we shall denote the rate of generation of potential energy due to diabatic processes by $[Q,P]$, the rate of dissipation of kinetic energy due to internal friction and mixing by $[K_1,D_i]$ and $[K_2,D_i]$, and the same due to the sea surface stress by $[K_1,D_s]$. Since the thermodynamical energy is considered only implicitly in this model, and since the dissipated kinetic energy is considered to be lost from the system, the use of Q, D_i or D_s in the above is purely symbolic.

By applying the ordinary procedure of deriving energy equations to (2.6) and (3.15) and then by grouping and transforming terms with the use of diagnostic equations of Sections 2 and 3, the equations governing $[K_1]$, $[K_2]$ and $[P]$ in the interval (r,r') are obtained in the following form:

$$\langle K_1]_r+[K_1]+[K_2\rangle_{r'}=[P,K_1]-[K_1,K_2]-[K_1,D_i]-[K_1,D_s], \tag{11.6}$$

$$\langle K_2]_r+[K_2]+[K_2\rangle_{r'}=[P,K_2]+[K_1,K_2]-[K_2,D_i], \tag{11.7}$$

$$\langle P]_r+[P]+[P\rangle_{r'}=[Q,P]-[P,K_1]-[P,K_2], \tag{11.8}$$

where

$$\langle K_1]=(\psi_0+\psi_1)v_1^2/2+\Lambda_1 v_1/r, \tag{11.9}$$

$$\langle K_2]=\psi_2 v_2^2/2+\Lambda_2 v_2/r, \tag{11.10}$$

$$\langle P]=g\{(\psi_0+\psi_1)(h_1+\epsilon h_2)+\psi_2(h_1+h_2)\}, \tag{11.11}$$

$$[Q,P]=\int g\sigma h_2 Q r dr, \tag{11.12}$$

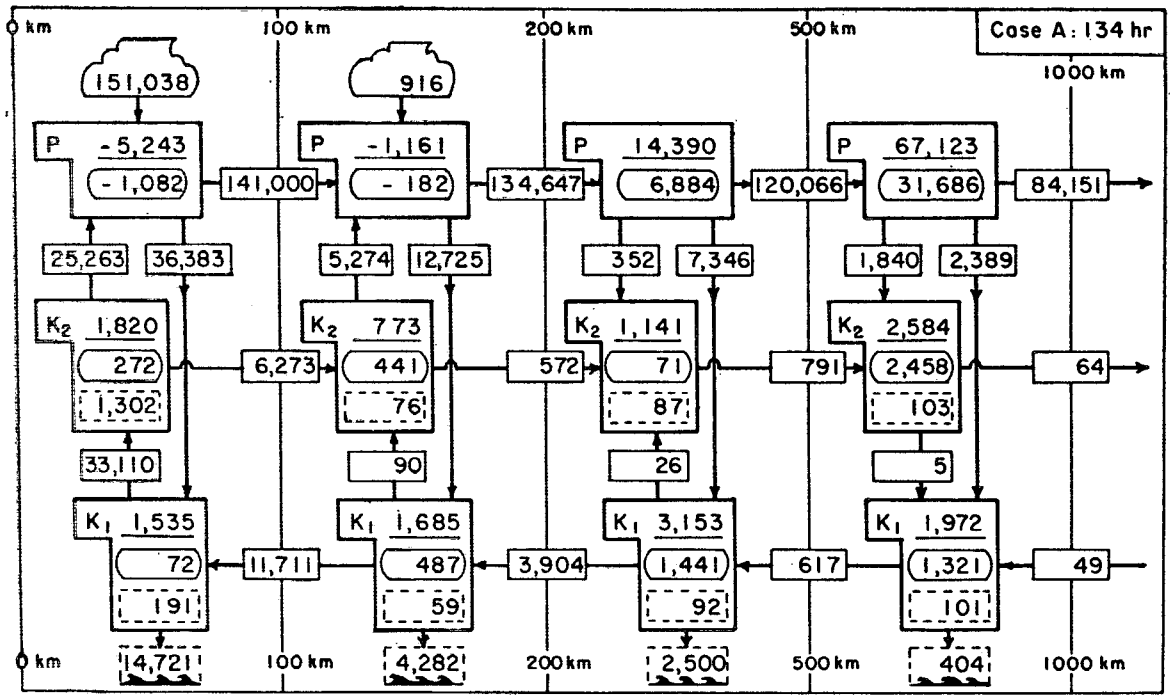

FIG. 8. The same as Fig. 7 but at $t=134$ hr (early mature stage).

$$[P,K_1]=\int(\psi_0+\psi_1)(\partial\phi_1/\partial r)rdr, \tag{11.13}$$

$$[P,K_2]=\int\psi_2(\partial\phi_2/\partial r)rdr, \tag{11.14}$$

$$[K_1,K_2]=\int\{(Q^+v_1^2-Q^-v_2^2)/2+\mu(v_1^2-v_2^2)/2\}rdr, \tag{11.15}$$

$$[K_1,D_i]=\int\{(Q^-+\mu)(v_1-v_2)^2/2+\lambda_1h_1r^2[\partial(v_1/r)/\partial r]^2\}rdr, \tag{11.16}$$

$$[K_2,D_i]=\int\{(Q^++\mu)(v_1-v_2)^2/2+\epsilon\lambda_2h_2r^2[\partial(v_2/r)/\partial r]^2\}rdr, \tag{11.17}$$

$$[K_1,D_s]=\int C_D|v_1|v_1^2rdr. \tag{11.18}$$

All the integrals in the above should be evaluated over the interval (r,r').

The first term on the right-hand side of (11.9) and (11.10) is the radial advective flux of kinetic energy, but the second term is the rate of work done by the frictional stress at the interval boundary. The vertical transport of kinetic energy, (11.15), also consists of the advection by the diabatic mass fluxes and the work by the frictional stress at the interface of the main layers. The radial transport of P includes both the advective flux and the rate of work done against the pressure at the interval boundary, although the two processes are not formally separated on the right-hand side of (11.11). The work done by the pressure gradient force is responsible for conversion of P to K_1 and K_2, (11.13) and (11.14), within the interval. Note that all the dissipation terms, (11.16)–(11.18), are always positive.

12. The energy budget and precipitation in the typical case

Numerical results of the energy budget in Case A are shown in Fig. 7 at the time the simulated cyclone is rapidly intensifying ($t=81$ hr); in Fig. 8, at the time the cyclone is entering the mature stage ($t=134$ hr); and in Fig. 9, at the late mature stage ($t=194$ hr). The underlined numbers indicate the amount of energy in each interval in the form of K_1, K_2 or P. (The amount shown for P is the difference from a standard value.) The rate of net change, $[K_1]$, $[K_2]$ or $[P]$, is shown in an oval outline. The internal dissipation, $[K_1,D_i]$ or $[K_2,D_i]$, is shown in a dashed-line rectangle. The surface dissipation, $[K_1,D_s]$, and the diabatic energy source, $[Q,P]$, are enclosed in self-explanatory outlines. (There is no radiative cooling in this numerical experiment). The rest of the conversion and transport terms are shown in a rectangle with an arrow indicating direction.

The nominal units for the numbers shown in Figs. 7–9 are 10^{13} m^5 sec^{-2} for K_1, K_2 and P, and 10^8 m^5 sec^{-3} for

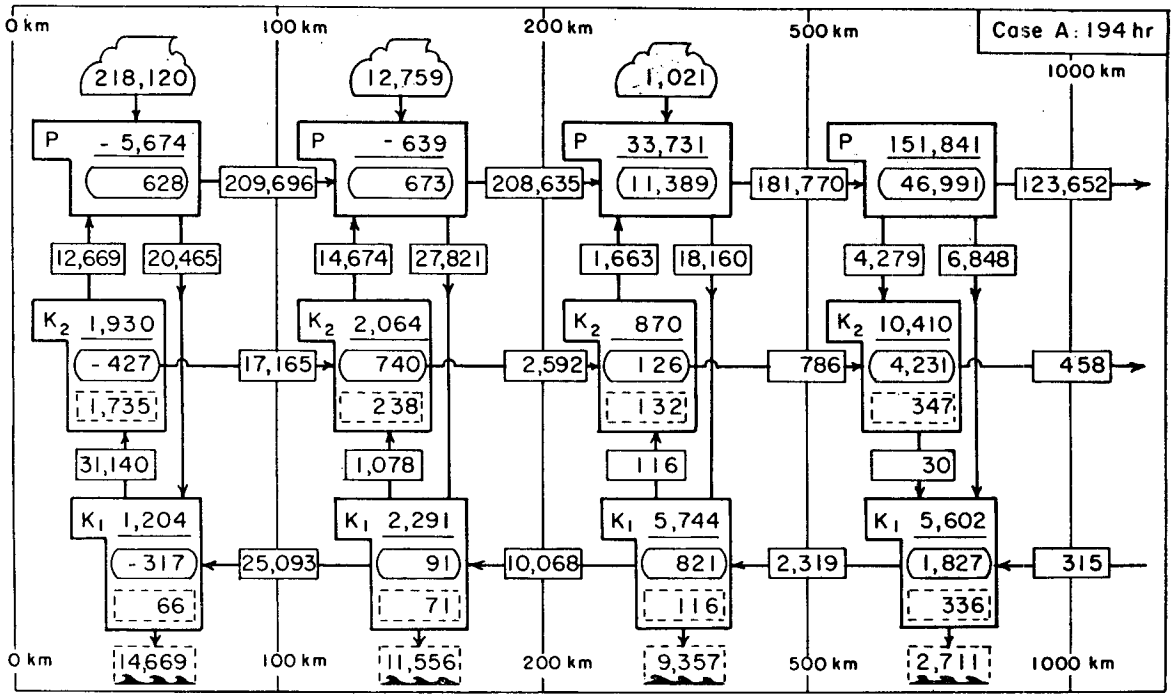

FIG. 9. The same as Fig. 7 but at $t=194$ hr (late mature stage).

all the others representing the time rates. The peculiar physical dimensions of these nominal units are due to the omission of the constant factor $2\pi\rho$ in the definition. In order to compare the computed energy budget with that of a tropical cyclone in nature, we may choose the otherwise arbitrary density ρ to be 10^{-3} ton m^{-3}, so that the mass in a unit vertical column of the model is approximately the same as that of the atmosphere. Then, one nominal unit for the amount of energy corresponds to 6.28×10^{13} joules, and one nominal unit for the time rate of energy corresponds to 6.28×10^{8} joules sec^{-1} (approximately one energy unit per day). In comparing numerical values in one radial interval with the corresponding values in another, it is important to take into account the areas, which are in the ratio 1:3:21:75 for the four intervals.

As shown in Figs. 7–9, the net change of the kinetic energy in the inner areas is due to a small balance among large contributing terms. From the energetics alone, it is difficult to explain why the balance should be positive or negative. The life cycle of the tropical cyclone appears to be more easily explainable along the line of the argument presented in the preceding section than by a simple argument based on magnitudes of the energy source or dissipation terms. However, taken chiefly as a diagnostic means, the balance sheets reveal an interesting interdependency among different parts of the cyclone.

The energy input to the system, $[Q,P]$, takes place almost exclusively in the innermost area (0–100 km), but very little is utilized to produce kinetic energy within the same area. As for the net production, $[P,K_1]+[P,K_2]$, the innermost area is most productive in terms of the yield per unit area, though not in terms of the total yield. However, the total dissipation of kinetic energy in the area actually exceeds the production. This is true even when the cyclone is rapidly intensifying (Fig. 7), and more conspicuously so at the later stage. On the other hand, utilizing part of the potential energy exported from the interior, the outer areas overproduce kinetic energy. Only by re-importing the surplus, does the intense circulation in the interior maintain itself.

It is of interest to determine the minimum radius of a self-contained area as far as kinetic energy production and dissipation are concerned. This radius may be about 500 km or less in Figs. 7 and 8, and between 500 and 1000 km in Fig. 9. In this sense, the computational limit of the model at 1000 km can be regarded as large enough for the present experiment. There is evidence to indicate that about 500 km must also be the minimum radius of the model if the angular momentum budget is not to be distorted too severely before the cyclone reaches the mature stage. It is emphasized, however, that a tropical cyclone should not be considered to be a closed system of such a radius. A substantial part of the diabatic energy input by the eye-wall convection is being exported out of the system at 1000 km, due to the use of the open boundary condition (4.5). If the system is literally closed at 500 km, or even at 1000 km, and all the energy is confined within the area, the system would warm up very rapidly in the absence of radiative cooling.

TABLE 2. Rainfall and latent heat release by implicit moist convection in Case A.

Time (hr)	q_0 (10^{-3})	q_2^*/q_0 (%)	F_q^+ (10^{10} ton day^{-1})	Condensation (10^{10} ton day^{-1})	Rainfall (0–100 km) (cm day^{-1})	Latent heat release (10^{19} joules day^{-1})
81	16.5	6.0	0.85	0.80	25.5	2.01
134	17.1	10.2	1.98	1.77	56.4	4.44
194	19.1	11.5	3.03	2.68	85.4	6.71

It is also interesting to note the origin of kinetic energy in the upper layer. In the lower layer, $[P,K_1]$ is positive everywhere due to the inflow down the pressure gradient. However, $[P,K_2]$ is positive only in the outer areas where the upper circulation is anticyclonic. In the inner cyclonic region of the upper layer, the outflow must proceed against the pressure gradient force and thus $[P,K_2]$ is negative. The only major process that can keep the upper cyclonic circulation going is the transport of kinetic energy, as well as the angular momentum, from the lower layer by the diabatic mass flux in the eye-wall convection, as shown by the large $[K_1,K_2]$ in the innermost area. In this experiment, the transport due to internal friction (λ and μ) is so small as to be negligible. Note that the consumption of kinetic energy by $[K_2,P]$ in the upper layer inside 200 km is even greater than $[K_1,D_s]$.

The rate of latent heat release in a mature tropical cyclone is estimated to be generally in the range of $2\text{–}6\times10^{19}$ joules day^{-1} (Dunn and Miller, 1964; Malkus and Riehl, 1960). At the rate of 4×10^{19} joules day^{-1}, the production of condensed water is 1.6×10^{10} tons day^{-1}, or 51 cm day^{-1} of precipitation if the rainfall is assumed to be uniform over an area of 100 km radius. On the other hand, $[Q,P]$ of the present model is found to be quite small. For example, after converting the nominal unit into the realistic unit, as explained above, we find $[Q,P]$ at 134 hr in Case A to be 0.82×10^{19} joules day^{-1}. If this energy input were interpreted as the rate of latent heat release, the precipitation would be 10.5 cm day^{-1} over the area of 100 km radius, too small for a mature cyclone. This discrepancy is apparently due to a misinterpretation of $[Q,P]$.

Although the thermodynamical energy of the moist air was duly taken into account in the modeling of moist convection in Section 5, the explicit effect of moist convection has not been incorporated in the model as a heat source. Instead, the effect has actually been introduced in the form of the vertical mass flux by making use of an analogy between the mass flux across an isentropic surface and the mass flux across an isopycnic surface. This is a device for matching the two fluid systems of different thermodynamical properties: the incompressible fluid system as the carrier of the cyclone scale fields and the atmospheric system for implicit formulation of the moist convection. Since the internal energy of air is missing in the former, the energy input of the model calculated from (11.12) is not the same as the amount of latent heat released by the implicit moist process. In view of the apparent success of the model in simulating many aspects of the tropical cyclone, the computed magnitude of $[Q,P]$ must be reasonable as the energy input to the analogue system. Nevertheless, this quantity is not observationally verifiable. The rate of latent heat release is obviously more interesting to us even though it is only implicitly connected to the energy budget of the simulated cyclone. An estimate of the latent heat release can be obtained in the following way.

The equivalent potential temperature χ_0 of the boundary layer is explicitly computed with the present model. The representative pressure p_0 of the layer at $z=h_0/2$ is also known. Therefore, the water vapor mixing ratio q_0 in this layer can be determined if the temperature T_0 is assumed. Since the horizontal temperature variation in the boundary layer is usually observed to be small, T_0 may be assumed to be constant (say, 24C at $z=h_0/2$) for this purpose. Once q_0 is known, the total upward flux F_q^+ of water vapor, which is being fed into convective clouds due to convergence of the boundary layer inflow, may be obtained by integrating $\rho q_0 w$ over the area where $w>0$; that is,

$$F_q^+=2\pi\rho\int_0^{r_x} q_0 w^+ r\,dr. \tag{12.1}$$

Practically all contributions to the integral come from a narrow band around the center where a sharp maximum of w is located.

The water vapor flux in the convective updraft may be augmented by entrainment of the ambient water vapor. While such entrainment can be estimated, it adds very little to F_q^+ since $\eta\simeq1$ in the convective area. However, in order to determine the rate of latent heat release in convective clouds, we must subtract from F_q^+ the uncondensed water vapor leaving the top of clouds. Since χ_2 is computed with the model, the mixing ratio q_2^* of the saturated air leaving the top of the clouds can be determined if the pressure at the average height of the clouds is assumed to be known. In accordance with our previous assumption in Section 6, we shall assume this pressure to be 300 mb.

At $t=134$ hr in Case A, for example, the average q_2^* in the convectively active region (25–60 km) is found to be 1.8×10^{-3}, while the average q_0 at the bottom of the clouds is 17.0×10^{-3}. Therefore, about 11% of F_q^+ ($=1.98\times10^{10}$ tons day^{-1}) is uncondensed and

TABLE 3. Energy budget of observed and simulated cyclones (units of 10^{11} joules sec^{-1}).

	Interval (km)	$[Q,P+I]$	$[P,K]$	$\langle K]$	$[K,D_s]$	$[K,D_i]$	$[K]$
			Limited storm area				
Palmén-Riehl (1957) A mean cyclone	28–222	5540	48.0	37.0	85.0	—	—
Riehl-Malkus (1961) Daisy, 1958							
25 August	0–148	1910	27.8	2.5	16.0	10.3	4.1
27 August	0–148	4400	68.3	34.7	32.4	66.0	4.6
Case A:							
$t=$ 81 hr	0–200	2320	23.2	3.6	14.3	2.9	9.6(10.0)
$t=134$ hr	0–200	5140	116.6	20.9	119.3	8.4	8.0(9.5)
$t=194$ hr	0 200	7770	131.5	46.9	164.7	13.2	0.5(0.9)
			Entire area of storm				
Palmén-Riehl (1957) A mean cyclone	28–666	5540	150.0	0.0	150.0	—	—
Case A:							
$t=$ 81 hr	0–1000	2320	40.3	0.0	15.9	3.5	20.9(21.3)
$t=134$ hr	0–1000	5140	191.5	−0.1	137.6	12.7	41.2(42.8)
$t=194$ hr	0–1000	7770	305.0	−0.9	240.5	19.1	44.5(45.0)

exported out of the convective region by the upper outflow. If all the condensed water is precipitated, the rate of rainfall, averaged over the area of 100 km radius, is found to be 56 cm day^{-1}, a reasonable figure for an intense tropical cyclone. Similar calculations have also been made at $t=81$ and 194 hr, the results of which are presented in Table 2.

It may be noted that the escape ratio q_2^*/q_0 sensitively depends on the assumed height of the average cloud top. If this height were assumed to be at the 400-mb level, the ratio, say at 134 hr, would be increased to 27%. The percentage assumed by Malkus and Riehl (1960) for a similar purpose was "25% or less." Therefore, it is possible that the estimates of latent heat release, rainfall, etc., in Table 2 have been overestimated. However, it is unlikely that these values are off by more than 15%.

Table 3 summarizes the energy budget of Case A in comparison with the results obtained from observed data by Palmén and Riehl (1957) and Riehl and Malkus (1961). Radial intervals (shown in km) in which the budget was calculated are not the same but are divided into two groups of approximately the same size. The symbol K without a subscript stands for the total kinetic energy, i.e., $K=K_1+K_2$, so that

$$[P,K]=[P,K_1]+[P,K_2],$$
$$\langle K]=\langle K_1]+\langle K_2], \text{ etc.}$$

The rate of latent heat release is denoted in this table by $[Q,P+I]$ and the values in Case A are taken from Table 2. All the numerical values in Table 3, except radii of intervals, are in units of 10^{11} joules sec^{-1}. In the last column, two values of $[K]$ are shown on each line of Case A to indicate the degree of accuracy of numerical integration; a further explanation will be given after the main features of the table are discussed below.

Comparing the energy budget of hurricane Daisy on 25 August with that of Case A at 81 hr (0–200 km, the top part of Table 3), we may note the remarkable similarity between them. Both the observed and the simulated cyclones were intensifying but still immature at the time. About two days later in either case, the cyclones attained their peak intensity. However, the discrepancy in the energy budget between Daisy on 27 August and Case A at 134 hr is considerable, particularly in terms of both production and dissipation of kinetic energy. Since the present experiment is not designed for simulating any particular tropical cyclone in nature, it is difficult to form an objective judgment on the significance of the discrepancy shown. However, as was noted by Riehl and Malkus (1961), the lowest level of aircraft observation for Daisy on 27 August was 620 mb and no ship was reporting within 100 n mi of the storm center. The discrepancy between the "observed" and the simulated cyclones may not be as decisive as it appears to be.

In regard to the energy budget over the entire storm area (the lower part of Table 3), the simulated cyclone in the early mature stage (at 134 hr) is found to be quite similar to the mean cyclone by Palmén and Riehl (1957) except for the net change $[K]$. The mean cyclone was assumed to be in a steady state. The simulated cyclone in Case A does not approach a steady state but the tangential winds in the outer area continue to increase even during the mature stage. The increase in terms of wind velocity is small in the outer area. However, as shown in Fig. 10, the increase in terms of the total kinetic energy is considerable.

In analogy with a thermodynamic engine, the efficiency of a tropical cyclone may be defined as the ratio of the total kinetic energy production to the total heat input or, in the present notation, as the ratio of $[P,K]$ to $[Q,P+I]$. Although the efficiency thus defined has no direct relation to intensification or growth characteristics of the cyclone, it has been a diagnostic parameter of traditional interest. The efficiency of the Palmén-Riehl cyclone (28–666 km) is 2.7%. The efficiency of the simulated cyclone in Case A (0–1000 km) is found to be 1.7, 3.7 and 3.9% at $t=81$, 134, and 194 hr, respectively.

Of the two values of $[K]$ given on each line of Case A in Table 3, the first is the rate of change of K which was determined from (11.6) and (11.7) as the residual after all the other terms in these equations were diagnostically calculated. The second value (in parentheses) is the rate of change which was determined from the difference between the kinetic energy at two consecutive time steps. The two values of $[K]$ should agree if there were no truncation errors due to the use of finite difference approximations both in time integration and in the computation of the energy budget. A major cause of this discrepancy is the truncation error of the prognostic equations in the vicinity of the eye wall, where the motion fields have a sharp peak. A more detailed analysis has shown that the computational error is concentrated mostly in the passive upper layer, so that possibly dangerous feedback effects of the truncation error on the energetically active process in the lower layers are fortunately kept minimal. This observation has actually been confirmed by repeating the numerical integration of Case A with the radial increment reduced by half ($\Delta r=2.5$ km) and with correspondingly smaller time increments. The discrepancy between the two values of $[K]$ was reduced to less than one-third, but almost no difference was found in other essential aspects of the simulated cyclone. Therefore, the computational accuracy in the time integration of the model appears to be quite adequate.

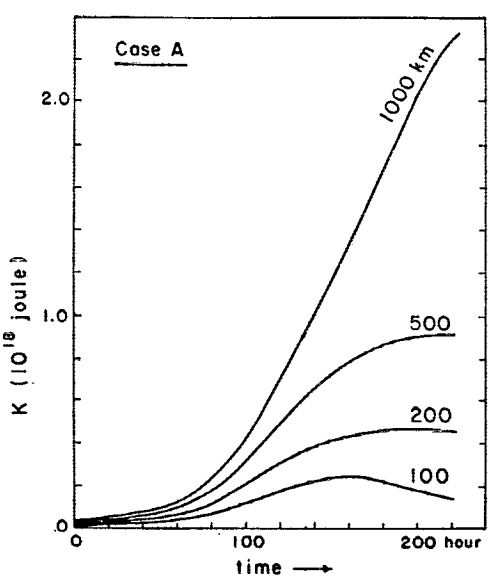

FIG. 10. Variation with time of the total kinetic energy of the computed cyclone in Case A for regions within radii of 100, 200, 500 and 1000 km.

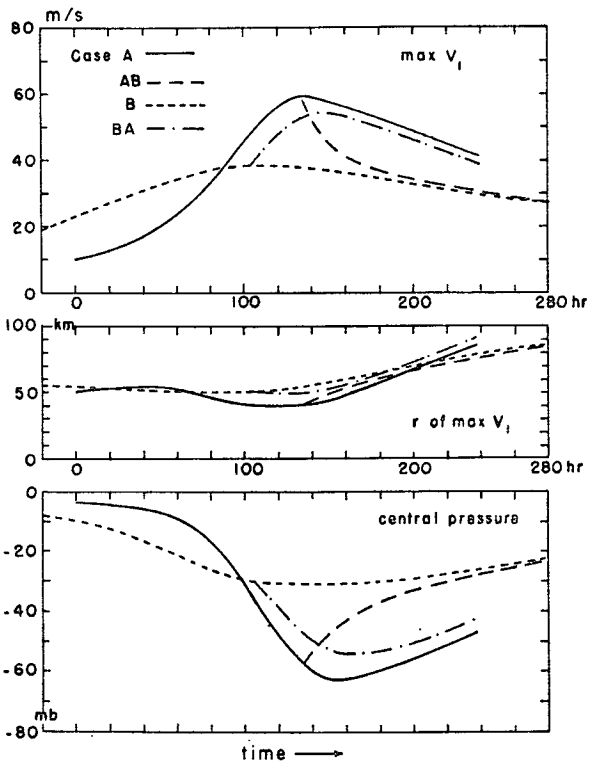

FIG. 11. Effects of the sea surface temperature on the intensity and size of computed cyclones. In Cases A and B, T_s is held constant at 27.5 and 25.6C, respectively. In Case AB, T_s is suddenly decreased from 27.5 to 25.6C at $t=134$ hr with an opposite change in Case BA at $t=104$ hr. The time origin of integration in Case B is at -100 hr (off the diagram).

13. Effects of the sea surface temperature

In a well-known study by Palmén (1948), it was shown that the oceanic regions of frequent tropical cyclone formation are climatologically associated with sea surface temperatures of about 26C or higher. There are also a number of studies indicating a close association of tropical cyclone intensity with sea surface temperature on shorter time scales (e.g., Fisher, 1958; Miller, 1958b; Perlroth, 1962). Therefore, it will be interesting to see how the simulated cyclone will behave for different values of the sea surface temperature, and two series of numerical experiments have been carried out for this purpose.

Results for the first series are summarized in Fig. 11. Case A with $T_s=27.5$C ($\bar{\chi}_s=30$K) is the same as before. In Case B, $T_s=25.6$C($\bar{\chi}_s=20$K) is assumed, but all the other parameters including the initial conditions are identical to those of Case A. Case AB is the same as

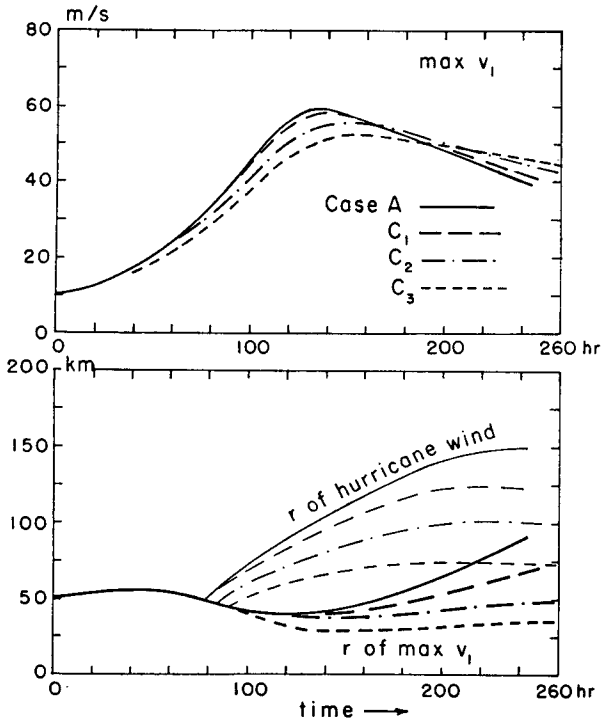

FIG. 12. Effects of sea surface temperature distribution on cyclone development. In Cases C_1, C_2 and C_3, T_s=25.6C for r>300 km, 25.6C for r>150 km, and 23.9C for r>150 km, respectively, while T_s=27.5C in the inner region in all cases. In Case A, the warm area extends to 1000 km.

Case A until max v_1 reaches a peak at t=134 hr; then T_s is suddenly decreased to 25.6C at all radii. Case BA is just the opposite: T_s suddenly increases from 25.6–27.5C when max v_1 of Case B is about to decline. For an easier comparison, the time origin of Case B is shifted to —100 hr on the time scale shown.

With the cold sea surface temperature, max v_1 in Case B barely manages to reach hurricane intensity, and the process takes twice as long as Case A, even though the moist convective instability η is initially the same in both cases. If lower values of χ_0, and thus smaller η, were initially assumed in Case B, the growth rate of the cyclone would have been much smaller. In Cases AB and BA, the rapid response of the cyclone intensity to a sudden change of T_s by only 2C is remarkable though not surprising. Although quantitative verification with observed cyclones is not available, a relaxation time constant of the order of one day or less does not seem unreasonable.

We have assumed in the above that the sea surface temperature is spatially uniform over the entire area, $r \leqslant 1000$ km. In real oceans, with the possible exception of the western Pacific Ocean, it is rather rare for the sea surface temperature of 27–28C to be found along the actual track of a tropical cyclone in a wide swath extending as far as 1000 km on either side of the track. Intense tropical cyclones do develop over much smaller bodies of warm water such as the Caribbean Sea and the Gulf of Mexico. It would be unrealistic if the intensification of the model cyclone really required so large an area of the warm ocean as assumed in Case A. On the other hand, the generally small size of Atlantic hurricanes compared with the huge size of some Pacific typhoons may well be due to the difference in area of the warm sea surface.

In order to examine how the simulated cyclone is affected by the size of the warm ocean area, the following series of experiments have been carried out. In Case C_1, it is assumed that T_s=27.5C inside r=300 km and 25.6C outside. In Case C_2, T_s=27.5C inside 150 km and 25.6C outside. In Case C_3, T_s=27.5C inside 150 km and 23.9C ($\bar{\chi}_s$=10K) outside. In all cases, T_s is kept constant with respect to time, and the initial conditions are the same as those of Case A. Results are summarized in Fig. 12.

In terms of max v_1, as shown in Fig. 12 (top), it makes very little difference whether the area of 27.5C extends to 1000 km (Case A) or is limited to 300 km (Case C_1). Even when the warm area is only 150 km in radius (Cases C_2 and C_3), the rate of intensification is still fairly rapid and the peak value of max v_1 exceeds 50 m sec^{-1}. However, in terms of the size of the cyclone, there are significant differences among the cases considered. As shown in Fig. 12 (bottom), both the radius of max v_1 and the outer limit of hurricane-force winds expand less when the warm inner area is smaller and the outside is colder.

The physical explanation for the differences in size is fairly obvious and is illustrated in Fig. 13. For instance, the center left diagram shows the radial distribution of χ_0 in Case C_1 (solid lines) in comparison with that of Case A (broken lines). Although the boundary layer inflow from the colder outer area (r>300 km) has lower values of χ_0, there is ample time in Case C_1 for the air to absorb heat and moisture from the warm inner sea before the inflow reaches the eye-wall convective region (r<60 km). As a result, there is practically no difference in the convective activity during the developing period (from 0 to about 140 hr) and only a slight difference during the mature stage.

On the other hand, the radial expansion of the cyclone becomes severely restricted when the warm sea extends only up to 150 km from the center, and particularly when the sea surface temperature in the outer area is so cold as in Case C_3. As shown in the center right diagram of Fig. 13, the original boundary-layer air with relatively high initial values of χ_0 is very rapidly exhausted and replaced largely by drier air subsiding from the layer above. However, in the region outside 150 km, the cold sea ($\chi_s \simeq$10K) cannot replenish the moisture to raise χ_0 above 10K. When the boundary layer inflow enters the warm inner area ($\chi_s \gtrsim$30K), χ_0 increases rather rapidly inward, although the subsidence of drier air is more intense in the interval between 50 and 150 km than on the outside. Nevertheless, the warm sea in this case is apparently too small to maintain a moist convective

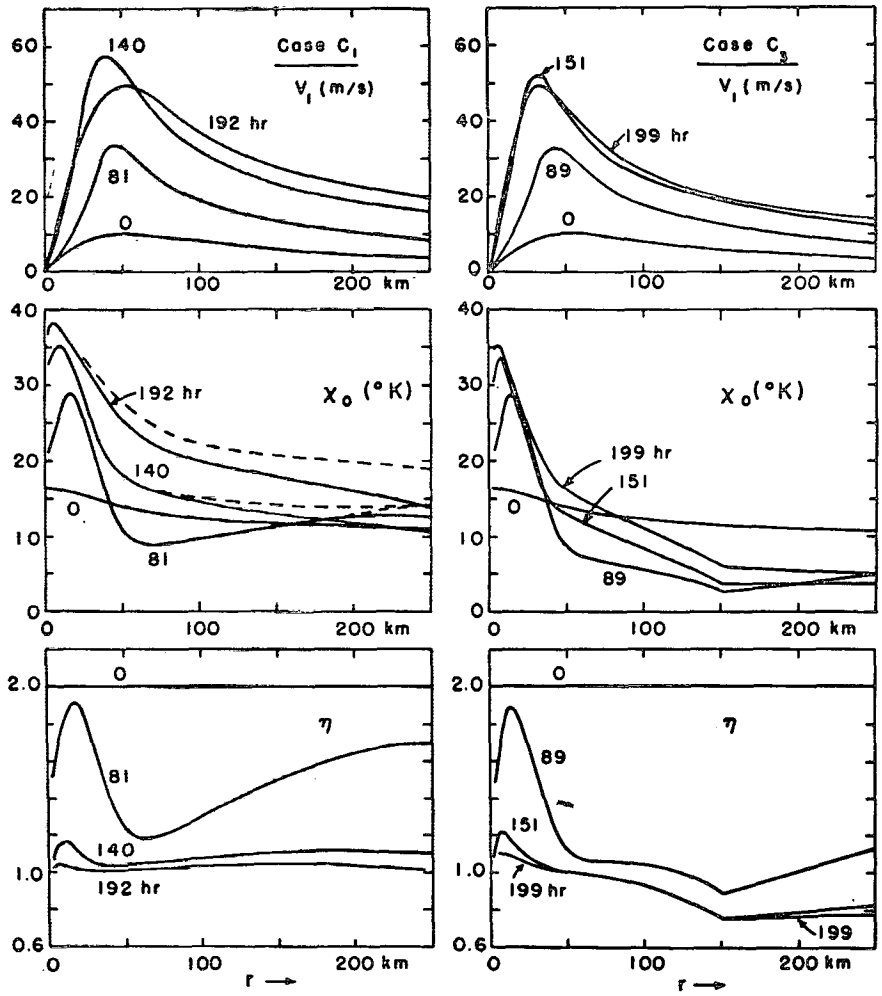

FIG. 13. Detailed comparison between Cases C_1 (left column) and C_3 (right column) in terms of radial distributions of v_1, χ_0 and η. Dashed lines in the center-left diagram represent χ_0 in Case A at comparable stages of cyclone development.

region of the same size as that of Case A or C_1. Furthermore, η outside about 50 km becomes less than unity due to the combined effect of upper warming and low values of χ_0, so that the region of unstable deep convection cannot expand during the mature stage. Consequently, very little change occurs in the radial distribution of tangential circulation after $t=151$ hr as shown in the top right diagram of Fig. 13.

In the case of a real tropical cyclone, the sea surface temperature distribution relative to the cyclone center depends both on the geographic distribution of sea surface temperature and on the cyclone track through the area. The present model, because of the assumption of axisymmetry, is not capable of simulating cyclone movement. However, the results of the experiments described in this section clearly indicate that the prediction of cyclone intensity and that of the cyclone track are not separable problems in nature. To a first approximation, the cyclone movement may be predicted by the so-called steering flow method (Sasaki and Miyakoda, 1954; Kasahara, 1960; Masuda, 1962; Morikawa, 1962; Kasahara and Platzman, 1963; and others), but further improvements in prediction will require the internal dynamics of the cyclone to be taken into account. On such a level of higher-order accuracy, it is quite possible, as Fisher (1958) attempted to show, that the sea surface temperature distribution becomes an important factor in determining the cyclone movement.

Although the sea surface temperature in the present model is considered as an external parameter, there is observational evidence that the sea surface temperature is lowered under the influence of a tropical cyclone (Fisher, 1958; Jordan, 1964; Leipper, 1967). Oceanographic observations by Leipper in the wake of hurricane Hilda, 1964, indicate that upwelling of the cold water from the depth of 50–60 m was responsible for a surface cooling of more than 5C in some areas along the path of the hurricane. Evaporative heat loss and

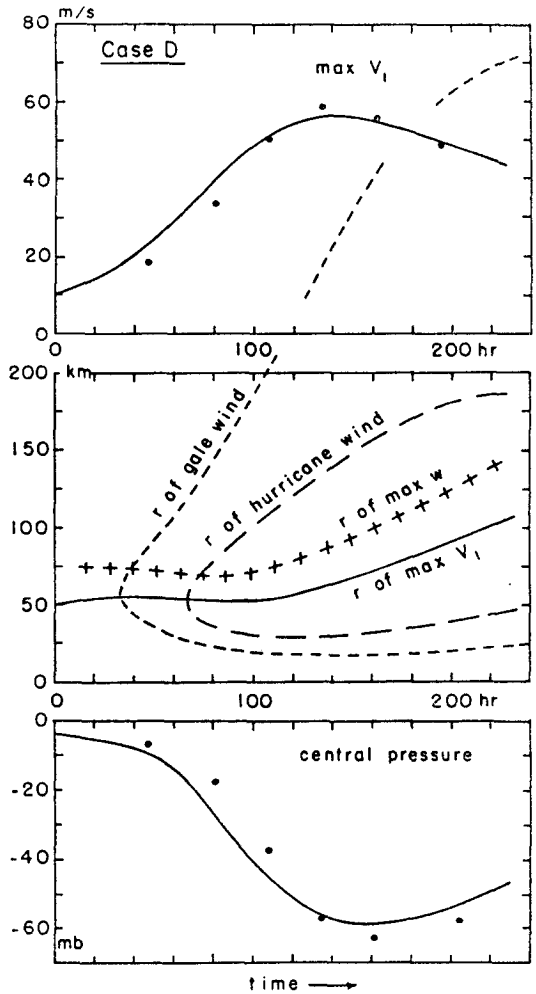

FIG. 14. Development of computed tropical cyclone in Case D with constant C_D and C_E. Results from Case A, in which these coefficients are a linear function of v_1, are indicated by dots (cf. Fig. 4).

vertical mixing may also contribute to surface cooling. Assuming a stationary hurricane with an empirical wind distribution, O'Brien and Reid (1967) and O'Brien (1967) have shown that the intense upwelling observed by Leipper is dynamically explainable as the action of wind stress at the surface of the stratified ocean.

What is still largely unknown is the feedback effect of the hurricane-induced surface cooling on the behavior of the hurricane. If a tropical cyclone is stationary, it will be weakened sooner or later. If a cyclone is moving, the feedback from intense upwelling can be neglected because of the time lag in oceanic response. However, quantitative discussion of the air-sea interaction in this regard will be extremely complicated since it involves not only the motion of the cyclone center but also the vertical temperature stratification in the ocean prior to the storm passage.

14. Experiments with C_D and C_E

The results of the foregoing experiments clearly demonstrate the importance of momentum, moisture and heat transfer between the atmosphere and ocean in a tropical cyclone. However, questions still remain concerning the quantitative formulation of eddy transfer processes. For example, the linear dependency of the drag coefficient on wind speed adopted in (9.1) is a plausible but still debatable assumption. Empirical data on evaporation from the sea under hurricane conditions are extremely scarce. Therefore, it is interesting to examine how sensitive the simulated cyclone is to the uncertainty in C_D and C_E.

Fig. 14 summarizes the results of Case D, in which C_D and C_E are assumed to be constant and equal, i.e.,

$$C_D = C_E = 1.5 \times 10^{-3}. \tag{14.1}$$

All the other specifications of Case D are identical to those of Case A. It may be noted that, if the 10-m level wind is assumed to be 80% of the gradient wind, the assumed value (14.1) corresponds to 2.3×10^{-3} for the drag coefficient in terms of the low level wind.

A comparison of Case D (Fig. 14) with Case A (Fig. 4) indicates differences in the radius of max v_1, the area of hurricane-force winds, and the variation of intensification rate. These differences are, at least qualitatively, explainable from the result of the linear analysis in Section 8, in which it was shown that the growth rate of a weak vortex is proportional to the coefficient of the surface friction. The constant C_D as given by (14.1) is larger than that in (9.1) at low wind speeds, and the relation is reversed at high wind speeds. However, if one considers that the crossing of (9.1) and (14.1) occurs at $v_1 = 16.7$ m sec^{-1}, a wind of less than gale force, it is rather surprising that the peak intensity in terms of either max v_1 or the central pressure differs very little in the two cases.

As discussed in Section 10, the time change of intensity is strongly affected by the variation of η, which was not taken into account in the linear analysis. Since the relative magnitude of C_E to C_D is an important factor in determining the variation of χ_0 and, thus, that of η, the apparent similarity of the intensification curves in Cases A and D seems to be a consequence of the assumption, $C_D = C_E$. In an experiment in which C_D was kept constant, at 1.5×10^{-3}, and C_E was assumed to increase with wind speed as in (9.1), max v_1 was found to exceed 95 m sec^{-1}. In the opposite case in which C_D increased but C_E remained constant, intensification stopped at max $v_1 = 45$ m sec^{-1}. Although such divergent behavior of C_D and C_E is unlikely to occur in nature, these experiments suggest that more definitive information on both coefficients is needed in quantitative simulation of tropical cyclones.

An interesting situation in which the assumption of $C_D = C_E$ will not hold may arise when a tropical cyclone makes landfall, and the heat and moisture supply from

the underlying surface is severely curtailed. As an idealized simulation of the landfall, let us assume that C_E is suddenly reduced to zero during the course of time integration. Results of such an experiment, Case AE, are shown in Figs. 15 and 16. Before $t=134$ hr, Case AE is identical to Case A; after that time, further supply of heat and moisture is completely cut off by assuming $C_E=0$ everywhere.

Although typical values of C_D over land are possibly one order of magnitude larger than those over the ocean, the specification of C_D in Case AE is unchanged during integration, so that C_D decreases as the wind speed drops after landfall in this experiment. The rapid decay of the cyclone shown in Figs. 15 and 16 is therefore not due to increased dissipation of kinetic energy, but rather to loss of oceanic supply of thermodynamic energy. Without a continuous supply of the latter, the simulated mature cyclone does not maintain its hurricane intensity more than 15 hr. If C_D had been increased at the landfall, the decay rate would have been greater. Although Case AE assumes C_E to vanish *everywhere*, such change occurring at more than a few hundred kilometers from the center does not immediately affect the decay process in the inner region. Therefore, a rapid decay similar to Case AE may be expected to occur when a tropical cyclone moves inland only a hundred kilometers or so from the coast. On the other hand, the

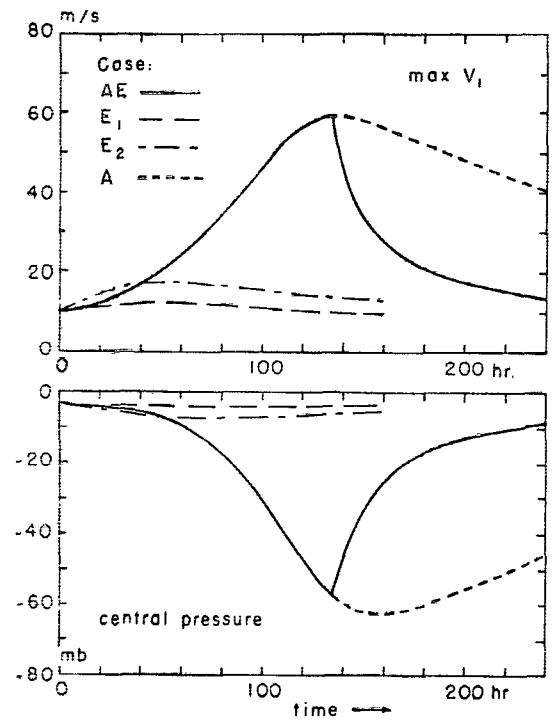

FIG. 15. Results of experiments demonstrating the importance of direct energy supply from the ocean to tropical cyclones. In Case AE, the energy supply to the Case A cyclone is suddenly stopped ($C_E=0$) at $t=134$ hr, to simulate landfall. In Cases E_1 and E_2, in which η is initially assumed to be 2.0 and 3.0, respectively, there is no energy supply from the ocean.

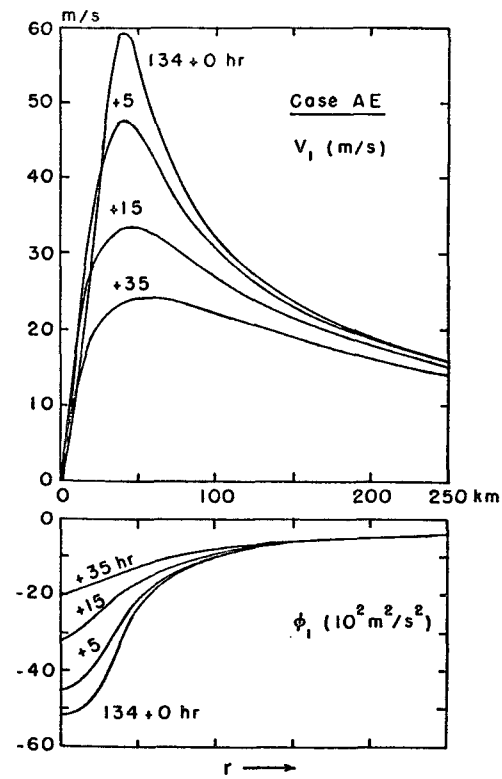

FIG. 16. Rapid decay of the computed tropical cyclone in Case AE following simulated landfall at $t=134$ hr. Radial distributions of v_1 (top) and ϕ_1 (bottom) are shown for 0, 5, 15, and 35 hr after landfall.

intensity of a cyclone staying more than 100 km offshore will be affected very little by the presence of the nearby land as long as the temperature of the coastal water is warm enough.

Fig. 15 also shows the results of two other experiments. In Case E_1, $C_E=0$ from the start of time integration; and in Case E_2, $\hat{\eta}=3$ in (9.4) and $C_E=0$. Otherwise, all specifications are identical to those of Case A. The purpose of these experiments is to see how far the weak initial vortex can grow by utilizing the latent heat already stored in the atmosphere. Even though the boundary layer in Case E_2 is initially almost saturated with water vapor, the unstable growth expected from the linear theory does not last more than 40 hr. In Case E_1, in which the initial relative humidity is about 85% ($\hat{\eta}=2$), intensification is negligible.

15. Experiments with initial conditions

We have assumed in this study that an incipient cyclone of some intensity is already given and the computations have been limited to the development of an incipient cyclone into a mature storm. However, since very little is actually known about structural details of the incipient cyclone, a degree of arbitrariness is unavoidable in prescribing initial conditions for numerical

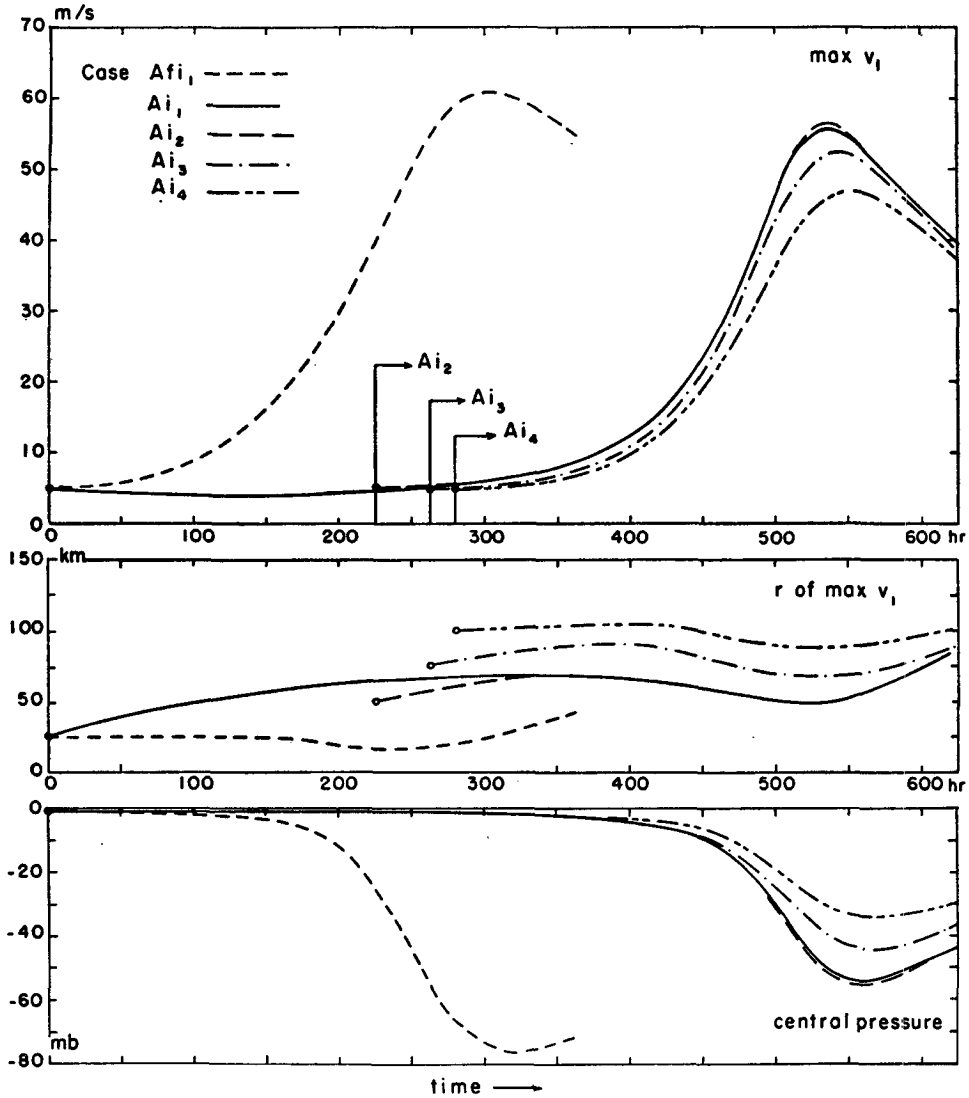

FIG. 17. Development of computed tropical cyclones from weak initial vortices of various sizes. Initially, max v_1 is 5 m sec^{-1} in all cases and the radii of max v_1 are 25, 50, 75 and 100 km in Cases Ai_1, Ai_2, Ai_3, and Ai_4, respectively. The time origin of integration in the last three cases is shifted as indicated for easier comparison. The lateral eddy viscosity is very small in Case Afi_1, which is otherwise identical to Case Ai_1 in specification.

experiments. In the preceding cases, the initial vortex was identical and was given by (9.2) and (9.3) with $\hat{v}=10$ m sec^{-1} and $\hat{r}=50$ km. In the following, we shall discuss a few experiments under different initial conditions, with results summarized in Fig. 17.

All the specifications in a series of four experiments, Ai_1 to Ai_4, are the same as those in Case A except for $\hat{v}$ and $\hat{r}$. The maximum tangential velocity $\hat{v}$ of the initial vortex is chosen in all four cases to be 5 m sec^{-1}. The radius $\hat{r}$ of maximum tangential wind is chosen to be 25, 50, 75 and 100 km in Cases Ai_1, Ai_2, Ai_3 and Ai_4, respectively. Case Afi_1 is different from Case Ai_1 only in the lateral eddy-viscosity coefficients, λ_1 and λ_2, which are chosen to be about 10^2 m^2 sec^{-1}, or one order of magnitude smaller than the value assumed in all other cases. The time origin on the abscissas of Fig. 17 is that of Cases Ai_1 and Afi_1. The time origins of the three other cases are shifted for easier comparison and are marked individually.

One of the notable features shown in Fig. 17 is a long "incubation" period in Case Ai_1; that is, during a period of about 300 hr (12 days), neither the central pressure nor max v_1 change very much. Due mainly to the diffusive effect of lateral friction, the radius of max v_1 gradually expands from about 25 to about 60 km during this period. However, the initial vortex is far from being simply dissipated. Although it is very weak initially, the unstable feedback between the cyclonic

circulation and the organized convective activity is operating from the start of integration; both v_1 and ψ_0 are actually increasing almost everywhere. As the vortex grows in size, the effectiveness of lateral friction is gradually reduced so that max v_1 itself eventually begins to increase.

The later stages of rapid intensification and maturation in Case Ai_1 are very similar to the corresponding stages in Case A; if the time origin in Fig. 4 is placed at $t=390$ hr on the time scale in Fig. 17, the corresponding curves of the two cases are found to parallel each other very closely. In this regard, Case Ai_2 is almost identical to Case Ai_1 and, thus, to Case A. The only significant difference between Cases Ai_1 and Ai_2 is the duration of the incipient stage as shown in Fig. 17.

In view of the arbitrariness in choosing initial conditions, it is reassuring that, at least in the above three cases, the intense cyclones evolving from the different initial conditions do not significantly differ from each other. However, great differences in length of the "incubation" period present a delicate problem with respect to the prediction of tropical cyclogenesis. In a real situation, oceanic regions of sufficiently high surface temperature are limited in size and atmospheric disturbances move across the regions. Such weak disturbances as assumed in Case Ai_1 may never reach the rapid intensification stage before moving out of a favored region.

The matter concerning the incipient stage is further complicated by changes in other factors. As shown in Fig. 17, the simulated cyclone in Case Afi_1 begins to intensify almost immediately by comparison with Case Ai_1. The only difference in specifications of the two experiments is in the lateral eddy viscosity. It may be noted that, although the intensity in terms of either max v_1 or the central pressure becomes stronger in this case than in Case Ai_1, the horizontal size of the cyclone remains much smaller. When compared at similar stages of development (in terms of max v_1), the total kinetic energy in Case Afi_1 is about one-third of the kinetic energy in Case Ai_1; the rates of total kinetic energy production and dissipation as well as the rate of rainfall are found to be small, correspondingly. However, results of other experiments (not illustrated) indicate that an early start of intensification, and the growth into a large-size cyclone, may be realized if the lateral eddy viscosity is not reduced while the drag coefficient at low speeds is increased, for instance by the use of (14.1).

The possibility that the size of a mature cyclone can be influenced by the size of the initial vortex is indicated by the results of Cases Ai_3 and Ai_4 in Fig. 17. Although wind speeds in these cases do not increase as much as in other cases, a larger area is affected, and the total kinetic energy of these cyclones is greater than that of smaller ones. If the experiment were to be made with a still larger initial vortex, the present model would allow an unrealistically large cyclone to develop. Since little is known about the structural details of tropical disturbances, it is not certain whether the choice of such a large initial vortex is, by itself, reasonable or not. However, the possibility of producing large cyclones with the model seems to indicate a flaw in the basic assumptions of the model. Under the axisymmetry assumption, for example, the eye-wall convection must occur uniformly around the cyclone center regardless of the radius of the eye. However, if this constraint is removed and the convective activity in one quadrant is allowed to become stronger than in others, the cyclone center may shift in that direction and a smaller eye may form around it.

There is reason to expect that elimination of the balance approximation from the boundary layer formulation would also bring a smaller eye. As was discussed by Ogura (1964), the nonlinear advective terms in the equation of radial motion are not quite negligible, in the frictional boundary layer of an intense tropical cyclone, by comparison with terms retained in the gradient wind relation. One probable effect of the advective terms is to allow the frictionally induced inflow to penetrate further inward than it does under the balance approximation, resulting in the eye-wall convection at a smaller radius. According to recent work by Yamasaki (to be published in *J. Meteor. Soc. Japan*) with a primitive-equation model, this effect appears to be quite real. However, since the eye of a computed cyclone with his model tends to disappear unless the initial vortex is assumed to be sufficiently large, the matter still remains to be investigated.

It may be noted that the assumed latitude for the Coriolis parameter also affects the size of computed cyclones with the model. Results of numerical experiments at various latitudes (between 15 and 25N) indicate that computed cyclones tend to grow smaller in size at lower latitudes. Since tropical cyclones in nature do not usually develop near the equator, it would be interesting to test the model at a very low latitude. However, because of the balance approximation with a constant Coriolis parameter, the present model is not suitable for such an experiment.

16. Conclusions

Compared to the complexity of real tropical cyclones, the present model is an extremely crude analog which is built on a system of hypotheses and approximations, few of which are really new in principle and many of which have been used previously in diagnostic studies of tropical cyclones. The purpose of experimenting with so simplified a model is to complement the existing observational knowledge of the tropical cyclone with a dynamically coherent frame of understanding. The model formulates the development of an incipient vortex into a mature tropical cyclone as a cooperative process between the cumulus-scale moist convection and the cyclone-scale circulation. Results of numerical

integration show that the model is capable of simulating the life cycle of a typical tropical cyclone with a remarkable degree of reality. Results also demonstrate that the supply of heat and moisture directly from a warm ocean is a crucial requirement for growth and maintenance of a tropical cyclone, a fact that characterizes the tropical cyclone as truly a creature of the tropical oceans. It may be concluded that, as an attempt to explain basic mechanisms of the tropical cyclone in simplest possible physical terms, the present model has achieved its primary goal.

In terms of quantitative accuracy, one weak assumption in the present model is the use of gradient winds in the boundary layer. This weakness can be removed by the use of a better diagnostic approximation or even by the use of primitive equations. However, in order to investigate the remaining problems of the tropical cyclone, the most restrictive assumption at present is probably the axisymmetry. Realistic simulation of the formation of an incipient cyclone in a weak synoptic disturbance, or prediction of the movement of a cyclone center for practical purposes, will require a three-dimensional description of synoptic-scale fields. Although a three-layer representation (including the boundary layer) of the cyclonic circulation appears to be adequate within the scope of the present study, a higher degree of vertical resolution is desirable in future investigations.

Finally, the importance of continued and possibly expanded efforts in collecting observational data from tropical cyclones at various stages cannot be emphasized enough. The need for better verification data will become urgent as numerical models continue to improve.

Acknowledgments. The research for this work was supported by the National Science Foundation under Grant GA-623 (continuation of GP-5192). The author wishes to thank Prof. J. Spar for helpful discussions and suggestions.

APPENDIX

Outline of Computational Procedure

Numerical integration of the model is performed with finite difference analogues of the model equations. The radial axis from $r=0$ to 1000 km is divided into 200 equal intervals separated by discrete points r_k, i.e.,

$$r_k=k\Delta r, \quad k=0, 1, \cdots, 200,$$

where $\Delta r=5$ km. Let k' denote the half odd integer associated with an integer k in such a way that $k'=k+\frac{1}{2}$. The middle point of the interval (r_k,r_{k+1}) is then given by

$$r_{k'}=k'\Delta r=(k+\tfrac{1}{2})\Delta r.$$

Variables such as v_j, ψ_j ($j=1$ and 2) and ψ_0 are defined at k points (r_k). These variables vanish at the center ($k=0$). Variables such as ϕ_j, h_j, η, Q^+ and all the χ's are defined at k' points ($r_{k'}$). The point of definition nearest to the center is at $r=2.5$ km.

The radial derivative of any k'-point variable, $\alpha_{k'}$, is approximated by a first-order finite difference quotient centered at a k point; that is,

$$(\partial\alpha/\partial r)_k\simeq\Delta_k\alpha/\Delta r,$$

where

$$\Delta_k\alpha\equiv\alpha_{k'}-\alpha_{k'-1}.$$

If the value of $\alpha_{k'}$ is required at a k point, an area-weighted average, $[\alpha]_k$, defined by

$$[\alpha]_k\equiv(r_{k'}\alpha_{k'}+r_{k'-1}\alpha_{k'-1})/2r_k,$$

is employed. An important exception to this rule is discussed below. For any k-point variable β_k, we may similarly define

$$\Delta_{k'}\beta\equiv\beta_{k+1}-\beta_k,$$
$$[\beta]_{k'}\equiv(r_{k+1}\beta_{k+1}+r_k\beta_k)/2r_{k'}.$$

In the above notation, derived functions such as ζ_j and w are defined as k'-point variables; thus,

$$\zeta_{j,k'}=\Delta_{k'}(v_jr)/(r_{k'}\Delta r),$$
$$w_{k'}=\Delta_{k'}\psi_0/(r_{k'}\Delta r).$$

We may thus write the diagnostic equation (3.19) as

$$\psi_{0,k}=(C_D|v_1|v_1r)_k/(f+[\zeta_1]_k).$$

In integrating the model as a marching problem, time extrapolation needs to be applied only to prediction of ϕ_j and χ_0. All other variables, including v_j, can be determined by solving the diagnostic equations. However, it has been found that a difference scheme for ζ_j in (4.1) must be chosen in such a way that the same scheme would make (3.15) computationally stable. Otherwise, the whole integration procedure becomes unstable even if (3.15) is not used explicitly for time extrapolation of v_j.

For the sake of concise description, let us consider an abbreviated system of equations which correspond to the original system of (3.1), (3.12), (3.15) and (4.1):

$$(f+v/r)v=\frac{\partial\phi}{\partial r}, \tag{A1}$$

$$\frac{\partial\phi}{\partial t}=g\frac{\partial\psi}{r\partial r}+G, \tag{A2}$$

$$\frac{\partial vr}{\partial t}=\frac{(f+\zeta)}{h}\psi+F, \tag{A3}$$

$$r\frac{\partial}{\partial r}\left(\frac{\partial\psi}{r\partial r}\right)-\frac{(f+2v/r)(f+\zeta)}{gh}\psi=B. \tag{A4}$$

At the nth time, t^n, we may assume that $v_k{}^n$ and $\phi_{k'}{}^n$ are already known and that the forcing terms,

$G_{k'}{}^n$, $F_k{}^n$ and $B_k{}^n$, are also computed from known fields. Time extrapolation from t^n to $t^{n+1}=t^n+\Delta t$ is carried out in the following way:

1) Calculate a *tentative* value of ψ_k at t^n, denoted by $\psi_k{}^*$, by linear extrapolation, i.e.,

$$\psi_k{}^*=2\psi_k{}^{n-1}-\psi_k{}^{n-2}. \tag{A5}$$

2) Calculate a *tentative* value of v_k at t^{n+1}, denoted by $v_k{}^*$, from (A.3) with the use of the uncentered upstream difference in ζ, i.e.,

$$\frac{(v_k{}^*-v_k{}^n)r_k}{\Delta t}=\frac{1}{[h]_k{}^n}(f+\langle\zeta\rangle_k{}^n)\psi_k{}^*+F_k{}^n, \tag{A6}$$

where

$$\langle\zeta\rangle_k{}^n\equiv\begin{cases}\Delta_{k'}(v^nr)/(r_k\Delta r), & \text{if } \psi_k{}^*>0,\\ \Delta_{k'-1}(v^nr)/(r_k\Delta r), & \text{if } \psi_k{}^*<0.\end{cases}$$

3) The finite-difference analog of (A4), which is to be solved for $\psi_k{}^n$, is written in the form

$$a_k\psi_{k+1}{}^n-b_k\psi_k{}^n+c_k\psi_{k-1}{}^n=(\Delta r)^2B_k{}^n, \tag{A7}$$

where

$$a_k\equiv r_k/r_{k'},\ c_k\equiv r_k/r_{k'-1},$$

$$b_k\equiv a_k+c_k+\frac{1}{g[h]_k{}^n}\left(f+\frac{2v_k{}^n}{r_k}\right)(f+\langle\zeta\rangle_k{}^{n,*}),$$

and

$$\langle\zeta\rangle_k{}^{n,*}\equiv\begin{cases}\dfrac{\Delta_{k'}(v^nr)+\Delta_{k'-1}(v^*r)}{2r_k\Delta r}, & \text{if } \psi_k{}^*>0\\ \dfrac{\Delta_{k'}(v^*r)+\Delta_{k'-1}(v^nr)}{2r_k\Delta r}, & \text{if } \psi_k{}^*<0\end{cases}$$

Under appropriate boundary conditions (Section 4), (A7) is easily solved by making use of the recurrence formulas described by Richtmyer (1957). It may be noted that the actual difference equation to be solved is a matrix equation corresponding to (4.1).

4) Calculate $\phi_{k'}{}^{n+1}$ from (A2) in the finite-difference form

$$\frac{\phi_{k'}{}^{n+1}-\phi_{k'}{}^n}{\Delta t}=g\frac{\Delta_{k'}\psi^n}{r_{k'}\Delta r}+G_{k'}{}^n. \tag{A8}$$

5) Obtain $v_k{}^{n+1}$ by solving (A1) in the finite-difference form

$$(f+v_k{}^{n+1}/r_k)v_k{}^{n+1}=\Delta_k\phi^{n+1}/\Delta r. \tag{A9}$$

As a method of predicting v, the use of the "split-level" centered difference, $\langle\zeta\rangle_k{}^{n,*}$, in (A3) leads to a difference scheme which is very similar to the two-step Lax-Wendroff scheme (Richtmyer, 1962). A linear analysis of this scheme indicates that $\delta\equiv U\Delta t/\Delta r<1$ is required for computational stability, where U denotes the absolute maximum of radial velocity (in the main layers) at any given time step. Since U may vary with time by an order of magnitude, Δt is programmed to vary automatically during time integration in such a way that $0.4<\delta^2<0.5$ is always satisfied.

It may be noted that (A5) is not applicable during the first two time steps following the start of integration or after the programmed changes of Δt. In these steps, $\psi_k{}^*$ is determined by solving (A7) with $[\zeta]_k{}^n$ for ζ. Prediction of χ_0 does not present any special problems requiring further discussion, except that the Δt determined above must be subdivided into smaller steps since the radial velocity is much greater in the boundary layer than in the main layers.

REFERENCES

Bolin, B., 1953: The adjustment of a non-balanced velocity field towards geostrophic equilibrium in a stratified fluid. *Tellus*, **5**, 373–385.

Charney, J. G., and A. Eliassen, 1964: On the growth of the hurricane depression. *J. Atmos. Sci.*, **21**, 68–75.

Dunn, G. E., 1951: Tropical cyclones. *Compendium of Meteorology*, Boston, Amer. Meteor. Soc., 887–901.

——, and B. I. Miller, 1964: *Atlantic Hurricanes*. Baton Rouge, State Univ. Press, 377 pp.

Eliassen, A., 1952: Slow thermally or frictionally controlled meridional circulation in a circular vortex. *Astrophys. Norv.*, **5**, No. 2, 60 pp.

Fisher, E. L., 1958: Hurricanes and the sea surface temperature field. *J. Meteor.*, **15**, 328–333.

Haque, S. M. A., 1952: The initiation of cyclonic circulation in a vertically unstable stagnant air mass. *Quart. J. Roy. Meteor. Soc.*, **78**, 394–406.

Jacobs, W. C., 1942: On the energy exchange between sea and atmosphere. *J. Marine Res.*, **5**, 37–66.

Jordan, C. L., 1958: Mean soundings for the West Indies area. *J. Meteor.*, **15**, 91–97.

——, 1964: On the influence of tropical cyclones on the sea surface temperature field. *Proc. Symp. Tropical Meteor.*, New Zealand Meteor. Service, 614–622..

Jordan, E. S., 1952: An observational study of the upper-wind circulation around tropical storms. *J. Meteor.*, **9**, 340–346.

Kasahara, A., 1960: The numerical prediction of hurricane movement with a two-level baroclinic model. *J. Meteor.*, **17**, 357–370.

——, 1961: A numerical experiment on the development of a tropical cyclone. *J. Meteor.*, **18**, 259–282.

——, and G. Platzman, 1963: Interaction of a hurricane with the steering flow and its effect upon the hurricane trajectory. *Tellus*, **15**, 321–335.

Kleinschmidt, E., 1951: Grundlagen einer Theorie der tropischen Zyklonen. *Arch. Meteor. Geophys. Bioklim.*, **A4**, 53–72.

Kuo, H. L., 1959: Dynamics of convective vortices and eye formation. *The Atmosphere and the Sea in Motion*, New York, Rockfeller Institute Press, 413–424.

——, 1961: Convection in conditionally unstable atmosphere. *Tellus*, **13**, 441–459.

——, 1965: On the formation and intensification of tropical cyclones through latent heat release by cumulus convection. *J. Atmos. Sci.*, **22**, 40–63.

Leipper, D. F., 1967: Observed ocean conditions and hurricane Hilda, 1964. *J. Atmos. Sci.*, **24**, 182–196.

Lilly, D. K., 1960: On the theory of disturbances in a conditionally unstable atmosphere. *Mon. Wea. Rev.*, **88**, 1–17.

Lorenz, E. N., 1960: Energy and numerical weather prediction. *Tellus*, **12**, 364–373.

Malkus, J. S., and H. Riehl, 1960: On the dynamics and energy transformations in steady state hurricanes. *Tellus*, **12**, 1–20.

Manabe, S., J. Smagorinsky and R. F. Strickler, 1965: Simulated climatology of a general circulation model with a hydrologic cycle. *Mon. Wea. Rev.*, **93**, 769–798.

Masuda, Y., 1962: On the general concept about the steering current in the baroclinic atmosphere and its application to numerical prediction of typhoon movement. *Proc. Intern. Symp. Numerical Weather Prediction*, Tokyo, Meteor. Soc. Japan, 341–348.

Miller, B. I., 1958a: On the momentum and energy balance of hurricane Helene (1958). National Hurricane Res. Proj. Rept. No. 53, 19 pp.

——, 1958b: On the maximum intensity of hurricanes. *J. Meteor.*, **15**, 184–195.

——, 1963: On the filling of tropical cyclones over land. National Hurricane Res. Proj. Rept. No. 66, 82 pp.

Mintz, Y., 1965: Very long-term global integration of the primitive equations of atmospheric motion. WMO Tech. Note No. 66, 141–167.

Morikawa, G. K., 1962: On the prediction of hurricane tracks using a geostrophic point vortex. *Proc. Intern. Symp. Numerical Weather Prediction*, Tokyo, Meteor. Soc. Japan, 349–360.

O'Brien, J. J., 1967: The non-linear response of a two-layer, baroclinic ocean to a stationary, axisymmetric hurricane: Part II. Upwelling and mixing induced by momentum transfer. *J. Atmos. Sci.*, **24**, 208–215.

——, and R. O. Reid, 1967: The non-linear response of a two-layer, baroclinic ocean to a stationary, axisymmetric hurricane: Part I. Upwelling induced by momentum transfer. *J. Atmos. Sci.*, **24**, 197–207.

Ogura, Y., 1964: Frictionally controlled, thermally driven circulation in a circular vortex with application to tropical cyclones. *J. Atmos. Sci.*, **21**, 610–621.

Ooyama, K., 1964: A dynamical model for the study of tropical cyclone development. *Geofis. Intern.*, **4**, 187–198.

——, 1966: On the stability of the baroclinic circular vortex: A sufficient criterion for instability. *J. Atmos. Sci.*, **23**, 43–53.

Östlund, H. G., 1967: Hurricane Tritium II: Air-sea exchange of water in Betsy 1965. Proj. Rept. ML 67043, Institute of Marine Sci., Univ. of Miami, 23 pp.

Palmén, E., 1948: On the formation and structure of tropical hurricane. *Geophysica*, **3**, 26–38.

——, and H. Riehl, 1957: Budget of angular momentum and energy in tropical cyclones. *J. Meteor.*, **14**, 150–159.

Perlroth, I., 1962: Relationship of central pressure of hurricane Ester (1961) and the sea surface temperature field. *Tellus*, **14**, 403–408.

Richtmyer, R. D., 1957: *Difference Methods for Initial-value Problems*. New York, Interscience Publishers, 101–104, 178–185.

——, 1962: A survey of difference methods for non-steady fluid dynamics. NCAR Tech. Notes 63–2, 25 pp.

Riehl, H., 1954: *Tropical Meteorology*. New York, McGraw–Hill, 392 pp.

——, 1963: Some relations between wind and thermal structure of steady state hurricanes. *J. Atmos. Sci.*, **20**, 276–278.

——, and J. S. Malkus, 1961: Some aspects of hurricane Daisy, 1958. *Tellus*, **13**, 181–213.

Roll, H. U., 1965: *Physics of the Marine Atmosphere*. New York, Academic Press, 426 pp.

Rosenthal, S. L., 1964: Some attempts to simulate the development of tropical cyclones by numerical methods. *Mon. Wea. Rev.*, **92**, 1–21.

Rossby, C.-G.. 1938: On the mutual adjustment of pressure and velocity distribution in certain simple current system. II. *J. Marine Res.*, **1**, 239–263.

Sasaki, Y., and K. Miyakoda, 1954: Prediction of typhoon tracks on the basis of numerical weather forecasting method. *Proc. UNESCO Symp. on Typhoons*, Japanese National Committee for UNESCO, 221–233.

Sawyer, J. S., 1947: Notes on the theory of tropical cyclones. *Quart. J. Roy. Meteor. Soc.*, **73**, 101–126.

Sheppard, P. A., 1958: Transfer across the earth's surface and through the air above. *Quart. J. Roy. Meteor. Soc.*, **84**, 205–224.

Simpson, R. H., and H. Riehl, 1958: Mid-tropospheric ventilation as a constraint on hurricane development and maintenance. *Bull. Amer. Meteor. Soc.*, **39**, 499.

Smagorinsky, J., S. Manabe and J. L. Holloway, 1965: Numerical results from a nine-level general circulation model of the atmosphere. *Mon. Wea. Rev.*, **93**, 727–768.

Syōno, S., 1953: On the formation of tropical cyclones. *Tellus*, **5**, 179–195.

——, 1962: A numerical experiment of the formation of tropical cyclones. *Proc. Intern. Symp. Numerical Weather Prediction*, Tokyo, Meteor. Soc. Japan, 405–418.

——, and M. Yamasaki, 1966: Stability of symmetrical motions driven by latent heat release by cumulus convection under the existence of surface friction. *J. Meteor. Soc. Japan*, Ser. II, **44**, 353–375.

Taylor, G. I., 1959: The present position in the theory of turbulent diffusion. *Advances in Geophysics*, Vol. 6, New York, Academic Press, 101–112.

Yanai, M., 1961: Dynamical aspects of typhoon formation. *J. Meteor. Soc. Japan*, Ser. II, **39**, 282–309.

——, 1964: Formation of tropical cyclones. *Rev. Geophys.*, **2**, 367–414.